

Manuscript prepared for Geosci. Model Dev.
with version 2014/09/16 7.15 Copernicus papers of the L^AT_EX class copernicus.cls.
Date: 4 December 2015

Using Reactive Transport Codes to Provide Mechanistic Biogeochemistry Representations in Global Land Surface Models: CLM-PFLOTTRAN 1.0

Guoping Tang¹, Fengming Yuan¹, Gautam Bisht^{1,2}, Glenn E. Hammond^{3,4}, Peter C. Lichtner⁵, Jitendra Kumar¹, Richard T. Mills⁶, Xiaofeng Xu^{1,7}, Ben Andre^{2,8}, Forrest M. Hoffman¹, Scott L. Painter¹, and Peter E. Thornton¹

¹Oak Ridge National Laboratory, Oak Ridge, Tennessee, United States

²Lawrence Berkeley National Laboratory, Berkeley, California, United States

³Pacific Northwest National Laboratory, Richland, Washington, United States

⁴Sandia National Laboratories, Albuquerque, New Mexico, United States

⁵OFM Research–Southwest, Santa Fe, New Mexico, United States

⁶Intel Corporation, Hillsboro, Oregon, United States

⁷San Diego State University, San Diego, California, United States

⁸National Center for Atmospheric Research, Boulder, Colorado, United States

Correspondence to: Peter E. Thornton (thorntonpe@ornl.gov), Scott L. Painter (paintersl@ornl.gov)

This manuscript has been authored by UT-Battelle, LLC under Contract No. DE-AC05-00OR22725 with the U.S. Department of Energy. The United States Government retains and the publisher, by accepting the article for publication, acknowledges that the United States Government retains a non-exclusive, paid-up, irrevocable, world-wide license to publish or reproduce the published form of this manuscript, or allow others to do so, for United States Government purposes. The Department of Energy will provide public access to these results of federally sponsored research in accordance with the DOE Public Access Plan(<http://energy.gov/downloads/doe-public-access-plan>).

Abstract. We explore coupling to a configurable subsurface reactive transport code as a flexible and extensible approach to biogeochemistry in land surface models; our goal is to facilitate testing of alternative models and incorporation of new understanding. A reaction network with the CLM-CN decomposition, nitrification, denitrification, and plant uptake is used as an example. We implement the reactions in the open-source PFLOTRAN code, coupled with the Community Land Model (CLM), and test at Arctic, temperate, and tropical sites. To make the reaction network designed for use in explicit time stepping in CLM compatible with the implicit time stepping used in PFLOTRAN, the Monod substrate rate-limiting function with a residual concentration is used to represent the limitation of nitrogen availability on plant uptake and immobilization. To achieve accurate, efficient, and robust numerical solutions, care needs to be taken to use scaling, clipping, or log transformation to avoid negative concentrations during the Newton iterations. With a tight relative update tolerance to avoid false convergence, an accurate solution can be achieved with about 50% more computing time than CLM in point mode site simulations using either the scaling or clipping methods. The log transformation method takes $60 \sim 100\%$ more computing time than CLM. The computing time increases slightly for clipping and scaling; it increases substantially for log transformation for half saturation decrease from 10^{-3} to $10^{-9} \text{ mol m}^{-3}$, which normally results in decreasing nitrogen concentrations. The frequent occurrence of very low concentrations (e.g. below nanomolar) can increase the computing time for clipping or scaling by about 20%; computing time can be doubled for log transformation. Caution needs to be taken in choosing the appropriate scaling factor because a small value caused by a negative update to a small concentration may diminish the update and result in false convergence even with very tight relative update tolerance. As some biogeochemical processes (e.g., methane and nitrous oxide production and consumption) involve very low half saturation and threshold concentrations, this work provides insights for addressing nonphysical negativity issues and facilitates the representation of a mechanistic biogeochemical description in earth system models to reduce climate prediction uncertainty.

1 Introduction

Land surface (terrestrial ecosystem) models (LSMs) calculate the fluxes of energy, water, and green-
35 house gases across the land-atmosphere interface for the atmospheric general circulation models for climate simulation and weather forecasting (Sellers et al., 1997). Evolving from the first generation “bucket”, second generation “biophysical”, and third generation “physiological” models (Seneviratne et al., 2010), current LSMs such as the Community Land Model (CLM) implement comprehensive thermal, hydrological, and biogeochemical processes (Oleson et al., 2013). The importance
40 of accurate representation of soil biogeochemistry in LSMs is suggested by the confirmation that the increase of carbon dioxide (CO_2), methane (CH_4), and nitrous oxide (N_2O) in the atmosphere since preindustrial time is the main driving cause of climate change, and interdependent water, carbon and nitrogen cycles in terrestrial ecosystems are very sensitive to climate changes (IPCC, 2013). In addition to ~ 250 soil biogeochemical models developed in the past ~ 80 years (Manzoni and Porporato,
45 2009), increasingly mechanistic models continue to be developed to increase the fidelity of process representation for improving climate prediction (e.g., Riley et al., 2014).

As LSMs usually hardcode the soil biogeochemistry reaction network (pools/species, reactions, rate formulae), substantial effort is often required to modify the source code for testing alternative models and incorporating new process understanding. Fang et al. (2013) demonstrated the use of a
50 reaction-based approach to facilitate implementation of the CLM-CN and CENTURY models and incorporation of the phosphorus cycle. Tang et al. (2013) solved the advection diffusion equation in CLM using operator splitting. In contrast, TOUGH-REACT, a reactive transport modeling (RTM) code, was used to develop multiphase mechanistic carbon and nitrogen models with many speciation and microbial reactions (Maggi et al., 2008; Gu and Riley, 2010; Riley et al., 2014), but it has not
55 been coupled to an LSM. PHREEQC was coupled with DayCent to describe soil and stream water equilibrium chemistry (Hartman et al., 2007). Coupling a RTM code with CLM will facilitate testing of increasingly mechanistic biogeochemical models in LSMs.

An essential aspect of LSMs is to simulate competition for nutrients (e.g., mineral nitrogen, phosphorus) among plants and microbes. In CLM, plant and immobilization nitrogen demands are cal-
60 culated independent of soil mineral nitrogen. The limitation of nitrogen availability on plant uptake and immobilization is simulated by a demand-based competition: demands are downregulated by soil nitrogen concentration (Oleson et al., 2013; Thornton and Rosenbloom, 2005). This avoids negative concentrations and does not introduce mass balance errors (Tang and Riley, 2015) as CLM uses explicit time stepping.

65 RTMs often account for limitation of reactant availability on reaction rates for each individual reaction to allow mechanistic representations and flexibility in adding reactions. For maximum robustness, some RTM codes support the use of fully implicit time stepping, usually employing a variant of the Newton-Raphson method. Negative concentration can be introduced during Newton-Raphson iterations, which is not physical and can cause numerical instability and errors (Shampine et al.,

70 2005). In our work with CLM, this is expected to worsen when we implement microbial reactions for methane and nitrous oxide consumption and production as the threshold, and half saturation is at or below nanomolar (10^{-9} M) level (Conrad, 1996). The redox potential Eh needs to be decreased to -0.35 V [oxygen concentration $< 10^{-22}$ M (Hungate, 1975)] for methanogens to grow (Jarrell, 1985).

75 Three methods are used to avoid negative concentration in RTM codes. One is to use the logarithm concentration as the primary variable (Bethke, 2007; Hammond, 2003; Parkhurst and Appelo, 1999). The other two either scale back the update vector (Bethke, 2007; Hammond, 2003) or clip the concentrations for the species that are going negative (Yeh et al., 2004; White and McGrail, 2005; Sonnenthal et al., 2014) in each iteration. Except that log transformation is more computationally demanding (Hammond, 2003), how these methods for enforcing nonnegativity affect computational accuracy and efficiency is rarely discussed.

80 As LSMs need to run under various conditions at the global scale for simulation duration of centuries, it is necessary to resolve accuracy and efficiency issues to use RTM codes for LSMs. The objective of this work is to explore some of the implementation issues associated with using 85 RTM codes in LSMs, with the ultimate goal being accurate, efficient, robust, and configurable representations of subsurface biogeochemical reactions in CLM. To this end, we develop an alternative implementation of an existing CLM biogeochemical reaction network using PFLOTRAN (Lichtner et al., 2015; Hammond et al., 2014); couple that model to CLM (we refer to the coupled model as CLM-PFLOTRAN); test the implementation at Arctic, temperate, and tropical sites; and examine 90 the implication of using scaling, clipping, and log transformation for avoiding negative concentrations. Although we focus on a number of carbon-nitrogen reactions implemented in PFLOTRAN and CLM, the critical numerical issue of avoiding negative concentrations has broader relevance as biogeochemical representations in LSMs become more mechanistic.

2 Methods

95 Among the many reactions in LSMs are the soil biogeochemical reactions for carbon and nitrogen cycles, in particular the organic matter decomposition, nitrification, denitrification, plant nitrogen uptake, and methane production and oxidation. The kinetics are usually described by a first-order rate modified by response functions for environmental variables (temperature, moisture, pH, etc.) (Bonan et al., 2012; Boyer et al., 2006; Schmidt et al., 2011). In this work, we use a network of the 100 CLM-CN decomposition (Bonan et al., 2012; Oleson et al., 2013; Thornton and Rosenbloom, 2005), nitrification, denitrification (Dickinson et al., 2002; Parton et al., 2001, 1996), and plant nitrogen uptake reactions (Fig. 1) as an example. The reactions and rate formulae are detailed in Appendix A.

2.1 CLM-PFLOTRAN biogeochemistry coupling

In CLM-PFLOTRAN, CLM can instruct PFLOTRAN to solve the partial differential equations for
105 energy (including freezing and thawing), water flow, and reaction and transport in the surface and subsurface. This work focuses on the PFLOTRAN biogeochemistry, with CLM solving the energy and water flow equations and handling the solute transport (mixing, advection, diffusion, and leaching). In each CLM time step, CLM provides production rates for Lit1C, Lit1N, Lit2C, Lit2N, Lit3C, Lit3N for litter fall; CWDC and CWDN for coarse woody debris production, nitrogen de-
110 position and fixation, and plant nitrogen demand; and specifies liquid water content, matrix potential and temperature for PFLOTRAN. PFLOTRAN solves ordinary differential equations for the kinetic reactions and mass action equations for equilibrium reactions and provides the final concentrations back to CLM.

The reactions and rates are implemented using the “reaction sandbox” concept in PFLOTRAN
115 (Lichtner et al., 2015). For each reaction, we specify a rate and a derivative of the rate with respect to any components in the rate formula, given concentrations, temperature, moisture content, and other environmental variables (see `reaction_sandbox_example.F90` in `pflotran-dev` source code for details). PFLOTRAN accumulates these rates and derivatives into a residual vector and a Jacobian matrix, and the global equation is discretized in time using the backward Euler method; the resulting
120 system of algebraic equations is solved using the Newton-Raphson method (Appendix B). A Krylov subspace method is usually employed to solve the Jacobian systems arising during the Newton-Raphson iterations, but, as the problems are relatively small in this study, we solve them directly via LU (lower upper) factorization.

Unlike the explicit time stepping in CLM, in which only reaction rates need to be calculated,
125 implicit time stepping requires evaluating derivatives. While PFLOTRAN provides an option to calculate derivatives numerically via finite-differencing, we use analytical expressions for efficiency and accuracy.

Many reactions can be specified in an input file, providing flexibility in adding various reactions with user-defined rate formulae. As typical rate formulae consist of first order, Monod, and inhibition
130 terms, a general rate formula with a flexible number of terms and typical moisture, temperature, and pH response functions is coded in PFLOTRAN. Most of the biogeochemical reactions can be specified in an input file, with a flexible number of reactions, species, rate terms, and various response functions without source code modification. Code modification is necessary only when different rate formulae or response functions are introduced. In contrast, the number of pools and reactions are
135 traditionally hardcoded in CLM. Consequently, any change of the pools, reactions, or rate formula may require source code modification. Therefore, the more general approach used by PFLOTRAN facilitates implementation of increasingly mechanistic reactions and tests of various representations with less code modification.

2.2 Mechanistic representation of rate-limiting processes

140 To use RTMs in LSMs, we need to make reaction networks designed for use in explicit time stepping LSMs compatible with implicit time stepping RTMs. The limitation of reactant availability on reaction rate is well represented by the first-order rate (Eqs. A1, A2, A5, A7): the rate decreases to zero as the concentration decreases to zero. A residual concentration $[CN_u]_r$ is often added to represent a threshold below which a reaction stops, for example to the decomposition rate (Eq. A1) as

$$145 \quad \frac{d[CN_u]}{dt} = -k_d f_T f_w ([CN_u] - [CN_u]_r). \quad (1)$$

Here CN_u is the upstream pool with 1:u as the CN ratio in mole; [] denotes concentration; and k_d , f_T , and f_w are the rate coefficient and temperature and moisture response functions, respectively. When CN_u goes below $[CN_u]_r$ in an iteration, Eq. (1) implies a hypothetical reverse reaction to bring it back to $[CN_u]_r$. The residual concentration can be set to zero to nullify the effect.

150 For the litter decomposition reactions [Appendix (R7), (R8), (R9)] that immobilize nitrogen (N), the nitrification reaction (R11) associated with decomposition to produce nitrous oxide, and the plant nitrogen uptake reactions (R13, R14), the rate formulae do not account for the limitation of the reaction rate by nitrogen availability. Mechanistically, a nitrogen limiting function needs to be added. For example, using the widely used Monod substrate limitation function (Fennell and Gossett, 155 1998), Eq.(1) becomes

$$\frac{d[CN_u]}{dt} = -k_d f_T f_w ([CN_u] - [CN_u]_r) \frac{[N] - [N]_r}{[N] - [N]_r + k_m}, \quad (2)$$

with half saturation k_m and a mineral nitrogen residual concentration $[N]_r$. In the case of $[N] - [N]_r = k_m$, the rate-limiting function is equal to 0.5. For $[N] \gg k_m$, Eq. (2) approximates zero order with respect to [N]. For $[N] \ll k_m$, Eq. (2) approximates first order with respect to [N]. The derivative of the 160 Monod term, $k_m([N] + k_m)^{-2}$, increases to about k_m^{-1} as the concentration decreases to below k_m . This represents a steep transition when k_m is small. The half saturation is expected to be greater than the residual concentration. When both are zero, the rate is not limited by the substrate availability.

To separate mineral nitrogen into ammonium (NH_4^+) and nitrate (NO_3^-), it is necessary to partition the demands between ammonium and nitrate for plant uptake and immobilization. If we simulate the 165 ammonium limitation on plant uptake with

$$R_a = R_p \frac{[NH_4^+]}{[NH_4^+] + k_m}, \quad (3)$$

the plant nitrate uptake can be represented by

$$R_n = (R_p - R_a) \frac{[NO_3^-]}{[NO_3^-] + k_m} = R_p \frac{k_m}{[NH_4^+] + k_m} \frac{[NO_3^-]}{[NO_3^-] + k_m}. \quad (4)$$

In this equation R_p , R_a , and R_n are the plant uptake rates for nitrogen, ammonium (R13), and 170 nitrate (R14). R_p is calculated in CLM and input to PFLOTRAN as a constant during each CLM

time step. Eq. (4) essentially assumes an inhibition of ammonium on nitrate uptake, which is consistent with the observation that plant nitrate uptake rate remains low until ammonium concentrations drop below a threshold (Eltrop and Marschner, 1996). However, the form of the rate expression will differ for different plants (Pfautsch et al., 2009; Warren and Adams, 2007; Nordin et al., 2001; 175 Falkengren-Grerup, 1995; Gherardi et al., 2013), which will require different representations in future developments.

CLM uses a demand-based competition approach (Appendix A, Section A5) to represent the limitation of available nitrogen on plant uptake and immobilization. It is similar to the Monod function except that it introduces a discontinuity during the transition between the zero and first-order rate. 180 Implementation of the demand-based competition in a RTM involves separating the supply and consumption rates for each species in each reaction and limiting the consumption rates if supply is less than demand after contributions from all of the reactions are accumulated. It involves not only the rate terms for the residual but also the derivative terms for the Jacobian. The complexity increases quickly when more species need to be downregulated (e.g., ammonium, nitrate, and organic nitrogen) and there are transformation processes among these species. It becomes challenging to separate, track, and downregulate consumption and production rates for an indefinite number of species, and calculation of the Jacobian becomes convoluted. In contrast, use of the Monod function with a residual concentration for individual reactions is easier to implement and allows more flexibility in adding reactions. 185

190 2.3 Scaling, clipping, and log transformation for avoiding negative concentration

Negative components of the concentration update ($\delta\mathbf{c}^{k+1,p+1}$ for iteration p from time step k to $k+1$ in a Newton-Raphson iteration) can result in negative concentration in some entries of $\mathbf{c}^{k+1,p}$ (Eq. B6), which is nonphysical. One approach to avoid negative concentration is to scale back the update with a scaling factor (λ) (Bethke, 2007; Hammond, 2003) such that

$$195 \quad \mathbf{c}^{k+1,p+1} = \mathbf{c}^{k+1,p} + \lambda \delta\mathbf{c}^{k+1,p+1} > 0, \quad (5)$$

where

$$\lambda = \min_{i=0,m} [1, \alpha \mathbf{c}^{k+1,p}(i) / \delta\mathbf{c}^{k+1,p+1}(i)] \quad (6)$$

for negative $\delta\mathbf{c}^{k+1,p+1}(i)$ with m as the number of species times the number of numerical grid cells and α as a factor with default value of 0.99. A second approach, used by RTM codes STOMP, 200 HYDROGEOCHEM 5.0, and TOUGH-REACT, is clipping [i.e., for any $\delta\mathbf{c}^{k+1,p+1}(i) \geq \mathbf{c}^{k+1,p}(i)$, $\delta\mathbf{c}^{k+1,p+1}(i) = \mathbf{c}^{k+1,p}(i) - \epsilon$ with ϵ as a small number (e.g., 10^{-20})]. This limits the minimum concentration that can be modeled.

A third approach, log transformation, also ensures a positive solution (Bethke, 2007; Hammond, 2003; Parkhurst and Appelo, 1999). It is widely used in geochemical codes for describing highly

205 variable concentrations for primary species such as H^+ or O_2 that can vary over many orders of magnitude as pH or redox state changes without the need to use variable switching. Instead of solving Eq. (B3) for \mathbf{c}^{k+1} using Eqs. (B4, B5, B6), this method solves for $(\ln \mathbf{c}^{k+1})$ (Hammond, 2003) with

$$\mathbf{J}_{\ln}(i,j) = \frac{\partial \mathbf{f}(i)}{\partial \ln(\mathbf{c}(j))} = \mathbf{c}(j) \frac{\partial \mathbf{f}(i)}{\partial \mathbf{c}(j)} = \mathbf{c}(j) \mathbf{J}(i,j), \quad (7)$$

210 $\delta \ln \mathbf{c}^{k+1,p+1} = -\mathbf{J}_{\ln}^{-1} \mathbf{f}(\mathbf{c}^{k+1,p}), \quad (8)$

and

$$\mathbf{c}^{k+1,p+1} = \mathbf{c}^{k+1,p} \exp [\delta \ln(\mathbf{c}^{k+1,p+1})]. \quad (9)$$

3 Tests, results, and discussions

The Newton-Raphson method and scaling, clipping, and log transformation are widely used and
215 extensively tested for RTMs, but not for coupled LSM-RTM applications. CLM describes biogeochemical dynamics within daily cycles for simulation durations of hundreds of years; the nitrogen concentration can be very low (mM to nM) while the carbon concentrations can be very high (e.g., thousands mol m⁻³ carbon in an organic layer); the concentrations and dynamics can vary dramatically in different locations around the globe. It is not surprising that the complex biogeochemical
220 dynamics in a wide range of temporal and spatial scales in CLM poses numerical challenges for the RTM methods. Our simulations reveal some numerical issues (errors, divergence, and small time step sizes) that were not widely reported. We identify the issues from coupled CLM-PFLOTRAN simulations and reproduce them in simple test problems. We examine remedies in the simple test problems and test them in the coupled simulations.

225 For Test 1, we start with plant ammonium uptake to examine the numerical solution for Monod function, and then add nitrification and denitrification incrementally to assess the implications of adding reactions. For Test 2, we check the implementation of mineralization and immobilization in the decomposition reactions. Thirdly, we compare the nitrogen demand partition into ammonium and nitrate between CLM and PFLOTRAN. With coupled CLM-PFLOTRAN spin-up simulations
230 for Arctic, temperate, and tropical sites, we assess the application of scaling, clipping, and log transformation to achieve accurate, efficient, and robust simulations. Spreadsheet and PFLOTRAN input files are provided as supplemental information (SI).

Our implementation of CLM soil biogeochemistry introduces mainly two parameters: half saturation (k_m) and residual concentration. A wide range of k_m values was reported for ammonium, nitrate,
235 and organic nitrogen for microbes and plants. The median, mean, and standard deviations range from 10~100, 50~500, and 10~200 μM , respectively (Kuzyakov and Xu, 2013). Reported residual concentrations are limited—likely because of the detection limits of the analytical methods—and are

considered to be zero (e.g., HØGh-Jensen et al., 1997). The detection limits are usually at the micro-molar level, while up to the nanomolar level was reported (Nollet and De Gelder, 2013). In Ecosys, 240 the k_m is 0.40 and 0.35 gN m⁻³, and the residual concentration is 0.0125 and 0.03 gN m⁻³ (Grant, 2013) for ammonium and nitrate for microbes. We start with $k_m = 10^{-6}$ M or mol m⁻³, and residual concentration = 10^{-15} M or mol m⁻³ for plants and microbes. To further investigate the nonphysical solution negativity for the current study and for future application for other reactants (e.g., H₂ and O₂) where the concentrations can be much lower, we examine k_m from 10^{-3} to 10^{-9} in our test 245 problems. The k_m is expected to be different for different plants, microbes, and for ammonium and nitrate. We do not differentiate them in this work as we focus on numerical issues.

3.1 Simple tests

3.1.1 Plant nitrogen uptake, nitrification, and denitrification

It was observed that plants can decrease nitrogen concentration to below the detection limit in hours 250 (Kamer et al., 2001). In CLM, the total plant nitrogen demand is calculated based on photosynthetized carbon allocated for new growth and the C:N stoichiometry for new growth allocation, and the plant nitrogen demand from the soil (R_p) is equal to the total nitrogen demand minus retranslocated nitrogen stored in the plants (Oleson et al., 2013). The demand is provided as an input to PFLO-TRAN. We use the Monod function to represent the limitation of nitrogen availability on uptake. We 255 examine the numerical solutions for the Monod equation at first. Incrementally, we add first-order reactions (e.g., nitrification, denitrification, and plant nitrate uptake) to look into the numerical issues in increasingly complex reaction networks.

Plant ammonium uptake (Test 1)

We consider the plant ammonium uptake reaction (R13) with a rate R_a

$$260 \quad \frac{d[\text{NH}_4^+]}{dt} = -R_a \frac{[\text{NH}_4^+]}{[\text{NH}_4^+] + k_m}. \quad (10)$$

Discretizing it in time using the backward Euler method for a time step size Δt , a solution is

$$[\text{NH}_4^+]^{k+1} = 0.5 \left[[\text{NH}_4^+]^k - k_m - R_a \Delta t \pm \sqrt{([\text{NH}_4^+]^k - k_m - R_a \Delta t)^2 + 4k_m [\text{NH}_4^+]^k} \right]. \quad (11)$$

Ignoring the negative root, $[\text{NH}_4^+]^{k+1} \geq 0$. Adding a residual concentration by replacing $[\text{NH}_4^+]$ with $[\text{NH}_4^+] - [\text{NH}_4^+]_r$, $[\text{NH}_4^+] \geq [\text{NH}_4^+]_r$. Namely, the representation of plant ammonium uptake 265 with the Monod function mathematically ensures $[\text{NH}_4^+]^{k+1} \geq [\text{NH}_4^+]_r$.

We use a spreadsheet to examine the Newton-Raphson iteration process for solving Eq. (10) and the application of clipping, scaling, and log transformation (SI test1.xlsx). When an overshoot gets the concentration closer to the negative than the positive root (Eq. 11), the iterations converge to the nonphysical negative semianalytical solution (spreadsheet case3). This can be avoided by using 270 clipping, scaling, or log transformation (spreadsheet case4, case6, case8).

Even though clipping avoids convergence to the negative solution, the ammonium consumption is clipped, but the PlantA production is not clipped (spreadsheet case5), violating the reaction stoichiometry. This results in mass balance errors for explicit time stepping (Tang and Riley, 2015). For implicit time stepping, additional iterations can resolve this violation to avoid mass balance error.

275 However, if a nonreactive species is added with a concentration of 1000 mol m^{-3} (e.g., soil organic matter pool 4 SOM4 in organic layer), the relative update $s_{norm_{rel}} = \|\delta\mathbf{c}^{k+1,p}\|_2 / \|\mathbf{c}^{k+1,p}\|_2$ decreases to 9.3×10^{-9} in the iteration (spreadsheet case5a). With a relative update tolerance [STOL, Eq. (B9)] of 10^{-8} , the iteration would be deemed converged. This false convergence may produce mass balance error. Satisfying the relative update tolerance criteria does not guarantee that the residual equations are satisfied (Lichtner et al., 2015). For this reason, we need a tight STOL to avoid this false convergence so that additional iterations can be taken to solve the residual equation accurately.

In contrast to clipping, scaling applies the same scaling factor to limit both ammonium consumption and PlantA production following the stoichiometry of the reaction (spreadsheet case6). However, if we add a production reaction that is independent of plant ammonium uptake, say nitrate deposition, which can come from CLM as a constant rate in a time step rather than an internally balanced reaction, scaling reduces the plant ammonium uptake to account for the availability of ammonium as we intend, but the nitrate deposition rate is also reduced by the same scaling factor even though it is not limited by the availability of either ammonium or nitrate (spreadsheet case7). Like clipping, this unintended consequence can be resolved in the subsequent iterations, and a loose

280 STOL may lead to false convergence and mass balance errors.

Small to zero concentration for ammonium and PlantA has no impact on the iterations for the clipping or scaling methods in this test. In contrast, a small initial PlantA concentration can cause challenges for the log transformation method even though PlantA is only a product. When it is zero, the Jacobian matrix is singular because zero is multiplied to the column corresponding to

285 PlantA (Eq. 7). An initial PlantA concentration of 10^{-9} can result in underflow of the exponential function (spreadsheet casea, as a 64-bit real number (“double precision”), is precise to 15 significant digits and has a range of e^{-709} to e^{709} in IEEE 754 floating-point representation (Lemmon and Schafer, 2005)). Clipping the update (say to be between -5 and 5) is needed to prevent numerical overflow or underflow. Like the cases with clipping without log transformation, clipping violates

290 reaction stoichiometry in the clipping iteration, and this violation needs to be resolved in subsequent iterations (spreadsheet caseb).

This simple test for the Monod function indicates that 1) Newton-Raphson iterations may converge to a negative concentration; 2) scaling, clipping, and log transformation can be used to avoid convergence to negative concentration; 3) small or zero concentration makes the Jacobian matrix

305 stiff or singular when log transformation is used, and clipping is needed to guard against overflow or underflow of the exponential function; 4) clipping limits the consumption, but not the corresponding production, violating reaction stoichiometry in the iteration; 5) production reactions with external

sources are inhibited in the iterations when scaling is applied, which is unintended; 6) additional iterations can resolve issues in 4) or 5); and 7) loose update tolerance convergence criteria may cause
 310 false convergence and result in mass balance errors for clipping and scaling.

Plant ammonium uptake and nitrification (Test 2)

Adding a nitrification reaction (R10) with a first-order rate to the plant ammonium uptake reaction (R13), Eq. (10) becomes

$$\frac{d[\text{NH}_4^+]}{dt} = -R_a \frac{[\text{NH}_4^+]}{[\text{NH}_4^+] + k_m} - k_{nitr} [\text{NH}_4^+] = -R_{at} - R_{nitr}. \quad (12)$$

315 A semianalytical solution similar to Eq. (11) can be derived for Eq. (12). With $J_{at} = dR_{at}/d[\text{NH}_4^+] = R_a k_m ([\text{NH}_4^+] + k_m)^{-2}$, and $J_{nitr} = dR_{nitr}/d[\text{NH}_4^+] = k_{nitr}$, the matrix equation Eq. (B5), becomes

$$\begin{bmatrix} 1/\Delta t + J_{at} + J_{nitr} & 0 & 0 \\ -J_{at} & 1/\Delta t & 0 \\ -J_{nitr} & 0 & 1/\Delta t \end{bmatrix} \begin{pmatrix} \delta[\text{NH}_4^+]^{k+1,1} \\ \delta[\text{PlantA}]^{k+1,1} \\ \delta[\text{NO}_3^-]^{k+1,1} \end{pmatrix} = - \begin{pmatrix} R_{at} + R_{nitr} \\ -R_{at} \\ -R_{nitr} \end{pmatrix}, \quad (13)$$

for the first iteration. As $R_{at} + R_{nitr} \geq 0$, the ammonium update is negative even when the ammonium concentration is not very low. The off-diagonal terms for PlantA and nitrate in the Jacobian matrix bring the negative ammonium update into the updates for PlantA and nitrate even though there is no reaction that consumes them. Specifically,

$$\frac{\delta[\text{PlantA}]^{k+1,1}}{\Delta t} = \frac{\frac{1}{\Delta t} + J_{nitr}}{\frac{1}{\Delta t} - J_{at} + J_{nitr}} R_{at} - \frac{J_{at}}{\frac{1}{\Delta t} + J_{at} + J_{nitr}} R_{nitr}, \quad (14)$$

$$325 \quad \frac{\delta[\text{NO}_3^-]^{k+1,1}}{\Delta t} = -\frac{J_{nitr}}{\frac{1}{\Delta t} + J_{at} + J_{nitr}} R_{at} + \frac{\frac{1}{\Delta t} + J_{at}}{\frac{1}{\Delta t} + J_{at} + J_{nitr}} R_{nitr}. \quad (15)$$

Depending on the rates (R_{at} , R_{nitr}), derivatives (J_{at} , J_{nitr}), and time step size Δt , the update can be negative for PlantA and nitrate, producing a zero order “numerical consumption,” in which the limitation of availability is not explicitly represented. This has implications for the scaling method.

The scaling factor (λ) is not only a function of the update; it is a function of the concentration (Eq. 330 6). If a negative update is produced for a zero concentration, the scaling factor is zero, decreasing the scaled update to zero. The iteration converges without any change to the concentrations, numerically stopping all of the reactions in the time step unless STOL is negative. We add the denitrification reaction with $R_{nitr} = 10^{-6} \text{ s}^{-1}$ to SI test1.xlsx case6 to create SI test2.xlsx to demonstrate that a small enough initial concentration relative to the negative update may numerically inhibit all of the 335 reactions as well. An update of $-6.6 \times 10^{-6} \text{ M}$ is produced for nitrate (spreadsheet scale1). When the initial nitrate concentration $[\text{NO}_3^-]_0$ is not too small, say 10^{-6} M , the solution converges to the semianalytical solution in six iterations. When $[\text{NO}_3^-]_0$ is decreased to 10^{-9} M , the relative update $snorm_{rel}$ is 9.2×10^{-10} . If $STOL = 10^{-9}$, the solution is deemed converged as Eq. (B9) is met,

but not to the positive semianalytical solution. The ammonium uptake and nitrification reactions are
340 numerically "inhibited" because the small scaling factor and a high concentration of a nonreactive species decreases the update to below STOL to reach false convergence. If we tighten STOL to 10^{-30} , the iterations continue, with decreasing nitrate concentration, λ , and $s_{norm_{rel}}$ by two orders of magnitude ($1-\alpha$ as default $\alpha = 0.99$) in each iteration, until $s_{norm_{rel}}$ reaches 10^{-30} (spreadsheet scale2). Unless STOL is sufficiently small, or MAXIT (the maximum number of iterations before
345 stopping the current iterations and cutting the time step) is small (Appendix B), false convergence is likely to occur for the scaling method. The impact of "numerical consumption" on clipping and log transformation is much less dramatic than the scaling method as the latter applies the same scaling factor to the whole update vector following stoichiometric relationships of the reactions to maintain mass balance, and the limiting concentration decreases by $(1 - \alpha)$ times in each iteration, with the
350 possibility of resulting in less than STOL relative update in MAXIT iterations.

In summary, this test problem demonstrates that 1) a negative update can be produced even for products during a Newton-Raphson iteration; and 2) when a negative update is produced for a very low concentration, a very small scaling factor may numerically inhibit all of the reactions due to false convergence even with very tight STOL.

355 *Plant uptake, nitrification, and denitrification (Test 3)*

The matrix and update equations with plant nitrate uptake and denitrification added to Test 2 are available in Appendix C. In addition to nitrate and PlantA, PlantN and the denitrification product nitrogen gas may have negative updates. In addition to the off-diagonal terms due to the derivative of plant uptake with respect to ammonium concentration, the derivative of plant uptake with respect
360 to nitrate concentration is added in the Jacobian matrix for PlantN (Eq. C1). As a result, a negative update for both ammonium and nitrate contributes to negative PlantN update through the two nonzero off-diagonal terms. Therefore, the likelihood for a negative update to PlantN is greater than PlantA as the former is influenced by more rates and derivatives. We add plant nitrate uptake and denitrification into SI test2.xlsx and assess the implications of increased reactions and complexity
365 in SI test3.xlsx. In addition to nitrate, this introduces a negative update for nitrogen gas in the first iteration (spreadsheet scale1). As the iterations resolve the balance between nitrite production from nitrification, and consumption due to plant uptake and denitrification, update to PlantN becomes negative and eventually leads to false convergence. The time step size needs to be decreased from 1800 to 15 s to resolve the false convergence (spreadsheet scale2). In contrast, the added reactions
370 have less impact on the clipping and log transformation methods.

3.1.2 Nitrogen immobilization and mineralization during decomposition (Test 4)

We examine another part of the reaction network: decomposition, nitrogen immobilization, and mineralization (Fig. 1). We consider a case of decomposing 0.2 M Lit1C + 0.005 M Lit1N to produce SOM1 with initial 4 μ M ammonium using the reactions (R2 and R7) in the CLM-CN reaction

375 network (Fig. 1). We use PFLOTRAN with a water-saturated grid cell with porosity of 0.25. At the beginning, Lit1 decreases and SOM1 increases sharply because the rate coefficient for Lit1 is 16 times that for SOM1 [Figs. 2(a), (b)]. As ammonium concentration decreases by orders of magnitude because of the faster immobilization than mineralization rate [Fig. 2 (c), (d)], Lit1 decomposition rate slows down to the level such that the immobilization rate is less than the mineralization rate.
 380 Namely, SOM1 decomposition controls Lit1 decomposition through limitation of mineralization on immobilization. As the immobilization rate decreases with decreasing Lit1, ammonium concentration rebounds after Lit1 is depleted. For k_m values of 10^{-6} , 10^{-9} , and 10^{-12} M, Lit1 and SOM1 dynamics are similar except for slight differences in the early transit periods, but the ammonium values are decreased to $\sim 10^{-8}$, 10^{-11} , and 10^{-14} M, respectively. Smaller k_m values result in lower
 385 ammonium concentrations, which have implications for the clipping, scaling, and log transformation methods as discussed in Tests 1–3.

3.1.3 Nitrogen demand partitioning between ammonium and nitrate

For comparison with CLM, we examine the uptake rate as a function of demands and available concentrations $f_{pi} = (R_a + R_n)/R_p$ as implemented in Eqs. (3) and (4). As an example, we consider uptake $R_p = 10^{-9}$ M s⁻¹ from a solution with various $[NH_4^+]$ and $[NO_3^-]$ for a 0.5 h time step. With CLM, $f_{pi} = 1$ when $[NH_4^+] + [NO_3^-] \geq R_p\Delta t$; otherwise, it decreases with decreasing $[NH_4^+] + [NO_3^-]$ (Fig. 3). The new representation (Eqs. 3, 4) is generally similar, with $f_{pi} = 1$ or 0 when $[NH_4^+]$ or $[NO_3^-] \gg k_m$ or $\ll k_m$. For the intermediate concentrations, f_{pi} in the new scheme is less than or equal to that in CLM because NH_4^+ “inhibits” NO_3^- uptake. The difference decreases 390 with decreasing k_m , apparently disappearing at $k_m = 10^{-10}$. Various levels of preferences of ammonium over nitrate uptake were observed for plants (Pfautsch et al., 2009; Warren and Adams, 2007; Nordin et al., 2001; Falkengren-Grerup, 1995; Gherardi et al., 2013), which is similar to microbial uptake of inorganic and organic nitrogen species (Fouilland et al., 2007; Kirchman, 1994; Kirchman and Wheeler, 1998; Middelburg and Nieuwenhuize, 2000; Veuger et al., 2004). CLM implies 395 a strong preference for ammonium over nitrate. For example, if ammonium is abundant, nitrate will not be taken by plants. The new scheme allows the level of preference to be adjusted by varying k_m ; more realistic representations can be implemented relatively easily.
 400

3.2 CLM-PFLOTRAN simulations

We test the implementation by running CLM-PFLOTRAN simulations for Arctic (US-Brw), temper-
 405 ate (US-WBW), and tropical (BR-Cax) AmeriFlux sites. The CLM-PFLOTRAN simulations are run in the mode in which PFLOTRAN only handles subsurface chemistry (decomposition, nitrification, denitrification, and plant nitrogen uptake). For comparison with CLM, 1) depth and O₂ availability impact on decomposition, 2) cryoturbation, 3) SOM transport, and 4) nitrogen leaching are ignored by setting 1) decomp_depth_efolding to 10⁶ m, and o_scalar to 1, and 2) cryoturb_diffusion, 3)

410 som_diffusion, and 4) sf_no3 and sf_sminn to 0 (Oleson et al., 2013). Spin-up simulations are used
because they are numerically more challenging as the simulations start far away from equilibrium.
In these site simulations, PFLOTRAN uses the same 10 layer grid for the 3.8 m one-dimensional
column as CLM. The simulation durations are 1000, 600, and 600 years for the Arctic, temperate,
and tropical sites, respectively. In the base case, $k_m = 10^{-6}$ mol m⁻³, and residual concentration
415 is 10⁻¹⁵ mol m⁻³. To assess the sensitivity of various preference levels for ammonium and nitrate
uptake and downregulation levels, we examine $k_m = 10^{-3}$ to 10⁻⁹ mol m⁻³. We evaluate how scal-
ing, clipping, and log transformation for avoiding negative concentrations influence accuracy and
efficiency. The simulations are conducted using the ORNL Institutional Cluster (OIC Phase5, an
SGI Altix with dual 8-core AMD Opterons per compute node) with CLM-PFLOTRAN (as well as
420 third-party libraries MPICH, PETSc, NetCDF, HDF5, etc.) compiled with gfortran 4.8.1 with the
“-O1” optimization level. Due to the small size of the simulations, our tests use only a single CPU
core.

3.2.1 Site descriptions

The US-Brw site (71.35N, 156.62W) is located near Barrow, Alaska. The mean annual temperature,
425 precipitation, and snowfall are -12 °C, 11 cm, and 69 cm, respectively (1971~2000) (Lara et al.,
2012). The landscape is poorly drained polygonized tundra. The maximum thaw depth ranges from
30 to 40 cm, and the snow-free period is variable in length but generally begins in early June and
lasts until early September (Hinkel and Nelson, 2003). The area is composed of several different rep-
resentative wet-moist coastal sedge tundra types, including wet sedges, grasses, moss, and assorted
430 lichens. The leaf area index (LAI) is ~1.1 (AmeriFlux data).

The US-WBW site (35.96N, 84.29W) is located in the Walker Branch Watershed in Oak Ridge,
Tennessee (Hanson and Wullschleger, 2003). The climate is typical of the humid southern Ap-
palachian region. The mean annual precipitation is ~139 cm, and the mean median temperature
is 14.5 °C. The soil is primarily Ultisols that developed in humid climates in the temperate zone
435 on old or highly weathered material under forest. The temperate deciduous broadleaf forest was
regenerated from agricultural land 50 years ago. LAI is ~ 6.2 (Hanson et al., 2004).

The BR-Cax site (-1.72N, -51.46W) is located in the eastern Amazon tropical rainforest. The
mean annual rainfall is between 200 and 250 cm, with a pronounced dry season between June and
November. The soil is a yellow oxisol (Brazilian classification latossolo amarelo) with a thick stony
440 laterite layer at 3~4 m depth (da Costa et al., 2010). The vegetation is evergreen broadleaf forest.
The LAI is 4~6 (Powell et al., 2013).

3.2.2 CLM-PFLOTRAN site simulation results

The site climate data from 1998 to 2006, 2002 to 2010, and 2001 to 2006 are used to drive the
spin-up simulation for the Arctic (US-Brw), temperate (US-WBW), and tropical (BR-Cax) sites, re-

445 spectsively. This introduces a multiyear cycle in addition to the annual cycle (Figs. 4, 5, 6). Overall, CLM-PFLOTRAN is close to CLM4.5 in predicting LAI and nitrogen distribution among vegetation, litter, SOM (soil organic matter), ammonium, and nitrate pools for the Arctic (Fig. 4), temperate (Fig. 5), and tropical (Fig. 6) sites. CLM4.5 does reach equilibrium earlier than CLM-PFLOTRAN. The maximum differences occur during the transient periods (200~400 years for the Arctic, and
450 50~70 years for the temperate and tropical sites) for SOMN (soil organic matter nitrogen), ammonium, and nitrate. This is not surprising as 1) the nitrogen demand competition scheme implemented in CLM-PFLOTRAN is different from that in CLM4.5 (Fig. 3); 2) the former solves the reaction network simultaneously while the latter does so sequentially (it resolves the plant uptake and decomposition first, then nitrification, then denitrification); and 3) the carbon nitrogen cycle is very
455 sensitive to the nitrogen competition representation. Close to steady state, both CLM4.5 and CLM-PFLOTRAN overpredict the LAI at the Arctic and temperate sites, and underpredict soil organic matter accumulation, which will be resolved in future work.

The Arctic site shows a distinct summer growing season (Fig. 4): LAI and VEGN (vegetation nitrogen) jump up at the beginning, then level off, and drop down at the end of the growing season
460 when LITN (litter nitrogen) jumps up due to litter fall. Ammonium and nitrate concentrations drop to very low levels at the beginning of the growing season and accumulate at other times. In addition to a longer growing season than the Arctic site, the temperate site shows more litter fall by the end of the growing season, as it is a temperate deciduous forest, which introduces immobilization demand that further lowers ammonium and nitrate concentrations [Fig. 5(e) inset]. The seasonality is much less
465 apparent in the tropical site than in the Arctic and temperate sites. LAI, VEGN, LITN, and SOMN accumulate with less seasonal variation to reach equilibrium.

Except for the tropical site where the higher k_m of 10^{-3} mol m $^{-3}$ results in lower immobilization, higher accumulation of LITN, and higher ammonium and nitrate concentrations during the spin-up (Fig. 6), the range of k_m values (10^{-6} and 10^{-9} mol m $^{-3}$) generally has limited impact on the overall
470 calculations except that the nitrogen concentrations drop lower with lower k_m values [e.g., inset in Figs. 4 (e), (f), 5 (e)]. The lack of sensitivity is because these very low concentrations do not make up a mass of nitrogen that is significant enough to influence the carbon and nitrogen cycle. However, as a small k_m means low concentrations (Test 4), and weak downregulation and steep transition between zero order and first order, it has implications on accuracy and efficiency of the numerical
475 solutions.

3.2.3 Accuracy and efficiency

Numerical errors introduced due to false convergence in clipping, scaling, or log transformation are captured in CLM when it checks carbon and nitrogen mass balance for every time step for each column and reports $\geq 10^{-8}$ g m $^{-2}$ errors. When log transformation is used, mass balance errors
480 are not recorded for the Arctic, temperate, and tropical sites with k_m values 10^{-3} , 10^{-6} , and 10^{-9}

mol m⁻³. The computing time for CLM-PFLOTTRAN is about 60~100% more than that of CLM (Table 1). This is not unreasonably high as the implicit method involves solving a Jacobian system for each Newton-Raphson step (Eq. B5), and log transformation converts the linear problem into a nonlinear one. The computational cost increases substantially with decreasing half saturation, which
485 is expected as a smaller half saturation requires smaller time step sizes to march through steeper transition between the zero and first-order rate in Monod function. Overall, log transformation is accurate, robust, and reasonably efficient.

Mass balance errors are reported for k_m values of 10^{-6} and 10^{-9} but not for 10^{-3} mol m⁻³ when clipping is applied. With $k_m = 10^{-3}$ mol m⁻³, the plant uptake and immobilization are inhibited at
490 a relatively high concentration so that nitrogen concentrations are high. With k_m decreasing from 10^{-6} to 10^{-9} mol m⁻³, nitrogen concentrations are lowered to a much lower level [Figs. 4, 5, 6, similar to Fig. 2(c)], increasing the likelihood of overshoot. Mass balance errors are recorded when the relative update is below STOL, preventing further iterations from resolving the violation of reaction stoichiometry introduced by clipping. The frequency of mass balance errors decreases with
495 increasing k_m , and decreasing STOL. Tightening STOL from 10^{-8} to 10^{-12} , the reported greater than 10^{-8} g m⁻³ mass balance errors are eliminated. The computing time is about 50% more than CLM, which is more efficient than log transformation (Table 1), particularly for $k_m = 10^{-9}$ mol m⁻³. Tightening STOL only slightly increases the computing time. Because clipping often occurs at very low concentrations, the reported mass balance errors are usually small ($\sim 10^{-8}$ gN m⁻² to $\sim 10^{-7}$
500 gN m⁻²), and do not have substantial impact on the overall simulation results.

The results for scaling are similar to clipping: mass balance errors are recorded for k_m values of 10^{-6} and 10^{-9} but not for 10^{-3} mol m⁻³; tightening STOL to 10^{-12} eliminates these errors; it takes about 50% more computing time than CLM. To examine the influence of low concentrations on the accuracy and efficiency of the scaling method, we conduct numerical experiments in which
505 we reset the nitrous oxide concentration produced from decomposition (reaction R11, rate Eq. A3) to 10^{-12} , 10^{-10} , or 10^{-8} mol m⁻³ in each CLM half hour time step for the tropical site for the first year. This can be used to calculate the nitrous oxide production rate from decomposition and feed back to CLM without saving the concentration for the previous time step. Overall, nitrogen is abundant in the first half year and then becomes limiting in the last five months [Fig. 6(e), (f),
510 inset]. We look into the daily ammonium cycles as an example during the nitrogen limiting period [day 250 to 260, Fig. 7(a)]. Every day the ammonium concentration increases with time due to deposition, but it drops when the plant nitrogen demand shots up. With a reset concentration of 10^{-8} mol m⁻³, the minimum nitrous oxide concentration for the ten layers is 10^{-8} mol m⁻³, and ammonium concentrations show two peaks followed by two drops due to the two plant uptake peaks
515 every day. Decreasing the reset concentration to 10^{-10} mol m⁻³, the minimum concentration drops to 10^{-12} , 10^{-14} , and 10^{-16} mol m⁻³, corresponding to 1, 2, and 3 scaling iterations with overshoot for nitrous oxide. These result in numerical “inhibition” of nitrogen rebound every day. It worsens

with further decrease of the reset concentration to 10^{-12} mol m $^{-3}$. This introduces mass balance errors as reported in CLM because the false convergence numerically inhibits all of the reactions
520 including nitrogen deposition and litter input from CLM to PFLOTRAN. Unlike clipping, these false convergences introduce excessive mass balance errors because of the inhibition of productions specified from CLM. If all of the reactions are internally balanced, false convergence does not result in mass balance errors.

The frequent negative update to nitrous oxide is produced because the rate for the nitrification
525 reaction (R11) is parameterized as a fraction of the net nitrogen mineralization rate to reflect the relationship between labile carbon content and nitrous oxide production (Parton et al., 1996). A Monod function is added to describe the limitation of ammonium concentration on nitrification. Calculation of the net mineralization rate involves all of the decomposition reactions, and the litter decomposition reactions bring in ammonium and nitrate limitation and ammonium inhibition
530 on nitrate immobilization. As a result, the off-diagonal terms for nitrous oxide in the Jacobian matrix corresponding to Lit1C, Lit1N, Lit2C, Lit2N, Lit3C, Lit3N, SOM1, SOM2, SOM3, SOM4, ammonium, and nitrate are nonzero. Negative updates to all of these species contribute to negative updates to nitrous oxide. Similar to Tests 2~3, a negative update to a low nitrous oxide concentration can decrease $s_{norm_{rel}}$ to below STOL, resulting in false convergence and mass balance errors.
535 While the empirical parameterization of nitrification rate as a function of net mineralization rate is conceptually convenient, it increases the complexity of the reaction network and computational cost due to the reduced sparsity of the Jacobian matrix. While we use nitrous oxide as an example here, similar results can be obtained for PlantN, PlantA, and nitrogen gas produced from denitrification, etc. Theoretically, the numerical "inhibition" of all reactions can be caused by negative updates to
540 very low concentrations for any species.

The numerical errors can be decreased and eliminated by decreasing STOL. Similar to Test 2 (SI test2.xlsx spreadsheet scale2), a small STOL can result in small $s_{norm_{rel}}$, then a very small STOL is needed. For the case of reset concentration 10^{-10} for the one year tropical site simulation, the numerical "inhibition" decreases with decreasing STOL and vanishes for the observed time
545 window when $STOL = 10^{-50}$ (Fig. 8), indicating the need for very small, zero, or even negative STOL to avoid false convergence. The impact of resetting nitrous oxide concentration on clipping and log transformation is less dramatic. Nevertheless, the computing time increases about 10% for clipping, and it doubles for the log transformation.

4 Summary and Conclusions

550 Global land surface models have traditionally represented subsurface soil biogeochemical processes using preconfigured reaction networks. This hardcoded approach makes it necessary to revise source code to test alternative models or to incorporate improved process understanding. We couple PFLO-

TRAN with CLM to facilitate testing of alternative models and incorporation of new understanding. We implement CLM-CN decomposition cascade, nitrification, denitrification, and plant nitrogen up-
555 take reactions in CLM-PFLOTRAN. We illustrate that with implicit time stepping using the Newton-Raphson method, the concentration can become negative during the iterations even for species that have no consumption, which need to be prevented by intervening in the Newton-Raphson iteration procedure.

Simply stopping the iteration with negative concentration and returning to the time stepping sub-
560 routine to cut time step size can avoid negative concentration, but may result in small time step sizes and high computational cost. Clipping, scaling, and log transformation can all prevent negative concentration and reduce computational cost. Our results reveal implications when the relative update tolerance (STOL) is used as one of the convergence criteria. While use of STOL improves efficiency in many situations, satisfying STOL does not guarantee satisfying the residual equation, and there-
565 fore it may introduce false convergence. Clipping reduces the consumption but not the production in some reactions, violating reaction stoichiometry. Subsequent iterations are required to resolve this violation. A tight STOL is needed to avoid false convergence and prevent mass balance errors. While the scaling method reduces the whole update vector following the stoichiometry of the reactions to maintain mass balance, a small scaling factor caused by a negative update to a small concentration
570 may diminish the update and result in false convergence, numerically inhibiting all reactions, which is not intended for productions with external sources (e.g., nitrogen deposition from CLM to PFLO-TRAN). For accuracy and efficiency, a very tight STOL is needed when the concentration can be very low. Log transformation is accurate and robust, but requires more computing time. The computational cost increases with decreasing concentrations, most substantially for log transformation.

575 Our CLM-PFLOTRAN spin-up simulations at Arctic, temperate, and tropical sites produce results similar to CLM4.5 and indicate that accurate and robust solution can be achieved with clipping, scaling, or log transformation. The computing time is 50~100% more than CLM4.5 for a range of half saturation values from 10^{-3} to 10^{-9} and a residual concentration of 10^{-15} for nitrogen. Because physical half saturation ranges from 10^{-5} to 10^{-6} M for nitrogen, and the detection limits are often
580 above 10^{-9} M, our results indicate that accurate, efficient, and robust solutions for current CLM soil biogeochemistry can be achieved using CLM-PFLOTRAN. We thus demonstrate the feasibility of using an open-source, general-purpose reactive transport code with CLM, enabling significantly more complicated and more mechanistic biogeochemical reaction systems.

An alternative to our approach of coupling LSMs with reactive transport codes is to code the so-
585 lution to the advection, diffusion, and reaction equations directly in the LSM. This has been done using explicit time stepping and operator splitting to simulate the transport and transformation of carbon, nitrogen, and other species in CLM (Tang et al., 2013). An advantage of our approach of using a community RTM to solve the advection-dispersion-reaction system is that the significant advances that the RTM community has made in the past several decades can be leveraged to better

590 represent the geochemical processes (e.g., pH, pE) in a systematic, flexible, and numerically reliable way. Given that a wide range of conditions may be encountered in any one global LSM simulation, it is particularly important to have robust solution methods such as fully implicit coupling of the advection-dispersion-reaction equations. As a next step, we hope CLM-PFLOTRAN will facilitate investigation of the role of the redox sensitive microbial reactions for methane production and consumption, and nitrification and denitrification reactions in ecological responses to climate change.

5 Code availability

PFLOTRAN is open-source software. It is distributed under the terms of the GNU Lesser General Public License as published by the Free Software Foundation either version 2.1 of the License, or any later version. It is available at <https://bitbucket.org/pfplotran>. CLM-PFLOTRAN is under development and will be made available according to the NGEE-Arctic Data Management Policies and Plans (<http://ngee-arctic.ornl.gov/content/ngee-arctic-data-management-policies-and-plans>). Before it becomes publicly available, please contact the corresponding authors to obtain access to the code.

6 Author contribution

G. B., B. A., R. M., J. K., and F. H. developed the CLM-PFLOTRAN framework that this work is built upon. F.Y., G.T., G. B., and X.X. added biogeochemistry to the CLM-PFLOTRAN interface. F. Y. proposed the nitrification and denitrification reactions and rate formulae. G. T., F. Y., and X. X. implemented the CLM soil biogeochemistry in PFLOTRAN under guidance of G. H., P. L., S. P., and P.T. G.T. prepared the manuscript with contributions from all co-authors. G. T., F. Y., G. B., and G.H. contributed equally to the work.

610 *Acknowledgements.* Thanks to Nathaniel O. Collier at ORNL for many discussions that contributed significantly to this work. Thanks to Kathie Tallant and Kathy Jones at ORNL for editing service. This research was funded by the U.S. Department of Energy, Office of Sciences, Biological and Environmental Research, Terrestrial Ecosystem Sciences and Subsurface Biogeochemical Research Program, and is a product of the Next-Generation Ecosystem Experiments in the Arctic (NGEE-Arctic) project. Development of CLM-PFLOTRAN was partially supported by the ORNL Laboratory Directed Research and Development (LDRD) program. ORNL is managed by UT-Battelle, LLC, for the U.S. Department of Energy under contract DE-AC05-00OR22725.

References

- Bethke, C. M.: Geochemical and biogeochemical reaction modeling, Cambridge University Press, 2007.
- Bonan, G. B., Hartman, M. D., Parton, W. J., and Wieder, W. R.: Evaluating litter decomposition in earth system models with long-term litterbag experiments: an example using the Community Land Model version 4 (CLM4), *Global Change Biology*, pp. 957–974, doi:10.1111/gcb.12031, <http://dx.doi.org/10.1111/gcb.12031>, 2012.
- Boyer, E. W., Alexander, R. B., Parton, W. J., Li, C., Butterbach-Bahl, K., Donner, S. D., Skaggs, R. W., and Grosso, S. J. D.: Modeling Denitrification in Terrestrial and Aquatic Ecosystems at Regional Scales, *Ecological Applications*, 16, 2123–2142, doi:10.1890/1051-0761(2006)016, [http://dx.doi.org/10.1890/1051-0761\(2006\)016](http://dx.doi.org/10.1890/1051-0761(2006)016), 2006.
- Conrad, R.: Soil microorganisms as controllers of atmospheric trace gases (H₂, CO, CH₄, OCS, N₂O, and NO), *Microbiological Reviews*, 60, 609–640, <http://mmbrr.asm.org/content/60/4/609.full.pdf>, 8987358[pmid] Microbiol Rev, 1996.
- da Costa, A. C. L., Galbraith, D., Almeida, S., Portela, B. T. T., da Costa, M., de Athaydes Silva Junior, J., Braga, A. P., de Gonçalves, P. H. L., de Oliveira, A. A. R., Fisher, R., Phillips, O. L., Metcalfe, D. B., Levy, P., and Meir, P.: Effect of 7 yr of experimental drought on vegetation dynamics and biomass storage of an eastern Amazonian rainforest, *New Phytologist*, 187, 579–591, doi:10.1111/j.1469-8137.2010.03309.x, <http://dx.doi.org/10.1111/j.1469-8137.2010.03309.x>, 2010.
- Dickinson, R. E., Berry, J. A., Bonan, G. B., Collatz, G. J., Field, C. B., Fung, I. Y., Goulden, M., Hoffmann, W. A., Jackson, R. B., Myneni, R., Sellers, P. J., and Shaikh, M.: Nitrogen Controls on Climate Model Evapotranspiration, *Journal of Climate*, 15, 278–295, doi:10.1175/1520-0442(2002)015, [http://dx.doi.org/10.1175/1520-0442\(2002\)015](http://dx.doi.org/10.1175/1520-0442(2002)015), 2002.
- Eltrop, L. and Marschner, H.: Growth and mineral nutrition of non-mycorrhizal and mycorrhizal Norway spruce (*Picea abies*) seedlings grown in semi-hydroponic sand culture, *New Phytologist*, 133, 469–478, doi:10.1111/j.1469-8137.1996.tb01914.x, <http://dx.doi.org/10.1111/j.1469-8137.1996.tb01914.x>, 1996.
- Falkengren-Grerup, U.: Interspecies differences in the preference of ammonium and nitrate in vascular plants, *Oecologia*, 102, 305–311, doi:10.1007/BF00329797, <http://dx.doi.org/10.1007/BF00329797>, 1995.
- Fang, Y., Huang, M., Liu, C., Li, H., and Leung, L. R.: A generic biogeochemical module for Earth system models: Next Generation BioGeoChemical Module (NGBGC), version 1.0, *Geosci. Model Dev.*, 6, 1977–1988, doi:10.5194/gmd-6-1977-2013, <http://www.geosci-model-dev.net/6/1977/2013>, gMD, 2013.
- Fennell, D. E. and Gossett, J. M.: Modeling the Production of and Competition for Hydrogen in a Dechlorinating Culture, *Environmental Science & Technology*, 32, 2450–2460, doi:10.1021/es980136l, <http://pubs.acs.org/doi/pdfplus/10.1021/es980136l>, 1998.
- Foulland, E., Gosselin, M., Rivkin, R. B., Vasseur, C., and Mostajir, B.: Nitrogen uptake by heterotrophic bacteria and phytoplankton in Arctic surface waters, *Journal of Plankton Research*, 29, 369–376, <http://plankt.oxfordjournals.org/content/29/4/369.abstract>, 2007.
- Gherardi, L. A., Sala, O. E., and Yahdjian, L.: Preference for different inorganic nitrogen forms among plant functional types and species of the Patagonian steppe, *Oecologia*, 173, 1075–1081, doi:10.1007/s00442-013-2687-7, <http://dx.doi.org/10.1007/s00442-013-2687-7>, 2013.

- Grant, R. F.: Modelling changes in nitrogen cycling to sustain increases in forest productivity under elevated atmospheric CO₂ and contrasting site conditions, *Biogeosciences*, 10, 7703–7721, doi:10.5194/bg-10-7703-2013, <http://www.biogeosciences.net/10/7703/2013/>, bG, 2013.
- Gu, C. and Riley, W. J.: Combined effects of short term rainfall patterns and soil texture on soil nitrogen cycling — A modeling analysis, *Journal of Contaminant Hydrology*, 112, 141–154, doi:10.1016/j.jconhyd.2009.12.003, <http://www.sciencedirect.com/science/article/pii/S0169772209001648>, 2010.
- Hammond, G. E.: Innovative Methods for Solving Multicomponent Biogeochemical groundwater Transport on Supercomputers, Thesis, University of Illinois at Urbana-Champaign, 2003.
- Hammond, G. E., Lichtner, P. C., and Mills, R. T.: Evaluating the performance of parallel subsurface simulators: An illustrative example with PFLOTRAN, *Water Resources Research*, 50, 208–228, doi:10.1002/2012WR013483, <http://dx.doi.org/10.1002/2012WR013483>, 2014.
- Hanson, P. and Wullschleger, S.: North American Temperate Deciduous Forest Responses to Changing Precipitation Regimes, Springer Verlag, 2003.
- Hanson, P. J., Amthor, J. S., Wullschleger, S. D., Wilson, K. B., Grant, R. F., Hartley, A., Hui, D., Hunt, J. E. R., Johnson, D. W., Kimball, J. S., King, A. W., Luo, Y., McNulty, S. G., Sun, G., Thornton, P. E., Wang, S., Williams, M., Baldocchi, D. D., and Cushman, R. M.: Oak forest carbon and water simulations: model intercomparisons and evaluations against independent data, *Ecological Monographs*, 74, 443–489, doi:10.1890/03-4049, <http://www.esajournals.org/doi/pdf/10.1890/03-4049>, 2004.
- Hartman, M. D., Baron, J. S., and Ojima, D. S.: Application of a coupled ecosystem-chemical equilibrium model, DayCent-Chem, to stream and soil chemistry in a Rocky Mountain watershed, *Ecological Modelling*, 200, 493–510, doi:10.1016/j.ecolmodel.2006.09.001, <http://www.sciencedirect.com/science/article/pii/S0304380006003942>, 2007.
- Hinkel, K. M. and Nelson, F. E.: Spatial and temporal patterns of active layer thickness at Circumpolar Active Layer Monitoring (CALM) sites in northern Alaska, 1995–2000, *Journal of Geophysical Research: Atmospheres*, 108, 8168, doi:10.1029/2001JD000927, <http://dx.doi.org/10.1029/2001JD000927>, 2003.
- Hungate, R.: The rumen microbial ecosystem, *Annual Review of Ecology and Systematics*, pp. 39–66, 1975.
- HØGh-Jensen, H., Wollenweber, B., and Schjoerring, J. K.: Kinetics of nitrate and ammonium absorption and accompanying H⁺ fluxes in roots of *Lolium perenne* L. and N₂-fixing *Trifolium repens* L, *Plant, Cell & Environment*, 20, 1184–1192, doi:10.1046/j.1365-3040.1997.d01-145.x, <http://dx.doi.org/10.1046/j.1365-3040.1997.d01-145.x>, 1997.
- IPCC: Climate Change 2013: The Physical Science Basis. Contribution of Working Group I to the Fifth Assessment Report of the Intergovernmental Panel on Climate Change, Cambridge University Press, Cambridge, United Kingdom and New York, NY, USA, doi:10.1017/CBO9781107415324, www.climatechange2013.org, 2013.
- Jarrell, K. F.: Extreme Oxygen Sensitivity in Methanogenic Archaeabacteria, *BioScience*, 35, 298–302, <http://bioscience.oxfordjournals.org/content/35/5/298.abstract>, 1985.
- Kamer, K., Kennison, R. L., and Fong, P.: Rates of inorganic nitrogen uptake by the estuarine green macroalgae *Enteromorpha intestinalis* and *Ulva expansa*, vol. 2003, pp. 130–141, 2001.

- 695 Kirchman, D. L.: The uptake of inorganic nutrients by heterotrophic bacteria, *Microbial Ecology*, 28, 255–271, doi:10.1007/BF00166816, <http://dx.doi.org/10.1007/BF00166816>, 1994.
- Kirchman, D. L. and Wheeler, P. A.: Uptake of ammonium and nitrate by heterotrophic bacteria and phytoplankton in the sub-Arctic Pacific, *Deep Sea Research Part I: Oceanographic Research Papers*, 45, 347–365, doi:10.1016/S0967-0637(97)00075-7, <http://www.sciencedirect.com/science/article/pii/S0967063797000757>, 1998.
- 700 Kuzyakov, Y. and Xu, X.: Competition between roots and microorganisms for nitrogen: mechanisms and ecological relevance, *New Phytologist*, 198, 656–669, doi:10.1111/nph.12235, <http://dx.doi.org/10.1111/nph.12235>, 2013.
- Lara, M. J., Villarreal, S., Johnson, D. R., Hollister, R. D., Webber, P. J., and Tweedie, C. E.: Estimated change 705 in tundra ecosystem function near Barrow, Alaska between 1972 and 2010, *Environmental Research Letters*, 7, 015 507, 2012.
- Lemmon, D. R. and Schafer, J. L.: *Developing Statistical Software in Fortran 95*, Statistics and Computing, Springer, 2005.
- Lichtner, P. C., Hammond, G. E., Lu, C., Karra, S., Bisht, G., Andre, B., Mills, R. T., and Jitu, K.: PFLO- 710 TRAN User Manual: A Massively Parallel Reactive Flow and Transport Model for Describing Surface and Subsurface Processes, Report, 2015.
- Maggi, F., Gu, C., Riley, W. J., Hornberger, G. M., Venterea, R. T., Xu, T., Spycher, N., Steefel, C., Miller, N. L., and Oldenburg, C. M.: A mechanistic treatment of the dominant soil nitrogen cycling processes: Model development, testing, and application, *Journal of Geophysical Research: Biogeosciences*, 113, G02 016, 715 doi:10.1029/2007JG000578, <http://dx.doi.org/10.1029/2007JG000578>, 2008.
- Manzoni, S. and Porporato, A.: Soil carbon and nitrogen mineralization: Theory and models across scales, *Soil Biology and Biochemistry*, 41, 1355–1379, doi:10.1016/j.soilbio.2009.02.031, <http://www.sciencedirect.com/science/article/pii/S0038071709000765>, 2009.
- Middelburg, J. J. and Nieuwenhuize, J.: Nitrogen uptake by heterotrophic bacteria and phytoplankton in the 720 nitrate-rich Thames estuary, *Marine Ecology Progress Series*, 203, 13–21, <http://www.int-res.com/abstracts/meps/v203/p13-21/>, 2000.
- Nollet, L. M. L. and De Gelder, L. S. P.: *Handbook of Water Analysis* (3rd Edition), CRC Press, 2013.
- Nordin, A., Högberg, P., and Näsholm, T.: Soil nitrogen form and plant nitrogen uptake along a boreal forest productivity gradient, *Oecologia*, 129, 125–132, doi:10.1007/s004420100698, <http://dx.doi.org/10.1007/s004420100698>, 2001.
- 725 Oleson, K., Lawrence, D., Bonan, G., Levis, S., Swenson, S., Thornton, P., Bozbayik, A., Fisher, R., Heald, C., Kluzek, E., Lamarque, J.-F., Lawrence, P., Lipscomb, W., Muszala, S., and Sacks, W.: Technical description of version 4.5 of the Community Land Model (CLM), *Ncar/tn-503+str*, ncar technical note, NCAR, doi:10.5065/D6RR1W7M, http://www.cesm.ucar.edu/models/cesm1.2/clm/CLM45_Tech_Note.pdf, 2013.
- Parkhurst, D. L. and Appelo, C.: User's guide to PHREEQC (Version 2): A computer program for speciation, batch-reaction, one-dimensional transport, and inverse geochemical calculations, *Water-Resources Investigations 99-4259*, USGS, 1999.

- Parton, W. J., Mosier, A. R., Ojima, D. S., Valentine, D. W., Schimel, D. S., Weier, K., and Kulmala, A. E.: Generalized model for N₂ and N₂O production from nitrification and denitrification, *Global Biogeochemical Cycles*, 10, 401–412, doi:10.1029/96GB01455, <http://dx.doi.org/10.1029/96GB01455>, 1996.
- 735 Parton, W. J., Holland, E. A., Del Grosso, S. J., Hartman, M. D., Martin, R. E., Mosier, A. R., Ojima, D. S., and Schimel, D. S.: Generalized model for NO_x and N₂O emissions from soils, *Journal of Geophysical Research: Atmospheres*, 106, 17 403–17 419, doi:10.1029/2001JD900101, <http://dx.doi.org/10.1029/2001JD900101>, 2001.
- 740 Pfautsch, S., Rennenberg, H., Bell, T. L., and Adams, M. A.: Nitrogen uptake by *Eucalyptus regnans* and *Acacia* spp. – preferences, resource overlap and energetic costs, *Tree Physiology*, 29, 389–399, <http://treephys.oxfordjournals.org/content/29/3/389.abstract>, 2009.
- Powell, T. L., Galbraith, D. R., Christoffersen, B. O., Harper, A., Imbuzeiro, H. M. A., Rowland, L., Almeida, S., Brando, P. M., da Costa, A. C. L., Costa, M. H., Levine, N. M., Malhi, Y., Saleska, S. R., Sotta, E., Williams, 745 M., Meir, P., and Moorcroft, P. R.: Confronting model predictions of carbon fluxes with measurements of Amazon forests subjected to experimental drought, *New Phytologist*, 200, 350–365, doi:10.1111/nph.12390, <http://dx.doi.org/10.1111/nph.12390>, 2013.
- Riley, W. J., Maggi, F., Kleber, M., Torn, M. S., Tang, J. Y., Dwivedi, D., and Guerry, N.: Long residence times of rapidly decomposable soil organic matter: application of a multi-phase, multi-component, and vertically resolved model (BAMS1) to soil carbon dynamics, *Geosci. Model Dev.*, 7, 1335–1355, doi:10.5194/gmd-7-1335-2014, <http://www.geosci-model-dev.net/7/1335/2014/>, gMD, 2014.
- 750 Schmidt, M. W. I., Torn, M. S., Abiven, S., Dittmar, T., Guggenberger, G., Janssens, I. A., Kleber, M., Kogel-Knabner, I., Lehmann, J., Manning, D. A. C., Nannipieri, P., Rasse, D. P., Weiner, S., and Trumbore, S. E.: Persistence of soil organic matter as an ecosystem property, *Nature*, 478, 49–56, <http://dx.doi.org/10.1038/nature10386>, 2011.
- 755 Sellers, P. J., Dickinson, R. E., Randall, D. A., Betts, A. K., Hall, F. G., Berry, J. A., Collatz, G. J., Denning, A. S., Mooney, H. A., Nobre, C. A., Sato, N., Field, C. B., and Henderson-Sellers, A.: Modeling the Exchanges of Energy, Water, and Carbon Between Continents and the Atmosphere, *Science*, 275, 502–509, doi:10.1126/science.275.5299.502, <http://www.sciencemag.org/content/275/5299/502.abstract>, 1997.
- 760 Seneviratne, S. I., Corti, T., Davin, E. L., Hirschi, M., Jaeger, E. B., Lehner, I., Orlowsky, B., and Teuling, A. J.: Investigating soil moisture–climate interactions in a changing climate: A review, *Earth-Science Reviews*, 99, 125–161, doi:10.1016/j.earscirev.2010.02.004, <http://www.sciencedirect.com/science/article/pii/S0012825210000139>, 2010.
- Shampine, L. F., Thompson, S., Kierzenka, J. A., and Byrne, G. D.: Non-negative solutions of ODEs, *Applied Mathematics and Computation*, 170, 556–569, doi:<http://dx.doi.org/10.1016/j.amc.2004.12.011>, <http://www.sciencedirect.com/science/article/pii/S0096300304009683>, 2005.
- Sonnenthal, E. L., Spycher, N., Xu, T., Zheng, L., Miller, N. L., and Pruess, K.: TOUGHREACT V3. 0-OMP Reference Manual: A Parallel Simulation Program for Non-Isothermal Multiphase Geochemical Reactive Transport, LBNL Report in preparation, Report, 2014.
- 770 Tang, J., Riley, W., Koven, C., and Subin, Z.: CLM4-BeTR, a generic biogeochemical transport and reaction module for CLM4: model development, evaluation, and application, *Geoscientific Model Development*, 6, 127–140, 2013.

- Tang, J. Y. and Riley, W. J.: Technical Note: A generic law-of-the-minimum flux limiter for simulating substrate limitation in biogeochemical models, *Biogeosciences Discuss.*, 12, 13 399–13 425, doi:10.5194/bgd-
775 12-13399-2015, <http://www.biogeosciences-discuss.net/12/13399/2015/>, bGD, 2015.
- Thornton, P. E. and Rosenbloom, N. A.: Ecosystem model spin-up: Estimating steady state conditions in a coupled terrestrial carbon and nitrogen cycle model, *Ecological Modelling*, 189, 25–48, doi:10.1016/j.ecolmodel.2005.04.008, <http://www.sciencedirect.com/science/article/pii/S0304380005001948>, 2005.
- 780 Veuger, B., Middelburg, J. J., Boschker, H. T. S., Nieuwenhuize, J., van Rijswijk, P., Rochelle-Newall, E. J., and Navarro, N.: Microbial uptake of dissolved organic and inorganic nitrogen in Randers Fjord, Estuarine, Coastal and Shelf Science, 61, 507–515, doi:10.1016/j.ecss.2004.06.014, <http://www.sciencedirect.com/science/article/pii/S0272771404001593>, 2004.
- Warren, C. R. and Adams, P. R.: Uptake of nitrate, ammonium and glycine by plants of Tasmanian wet eucalypt forests, *Tree Physiology*, 27, 413–419, <http://treephys.oxfordjournals.org/content/27/3/413.abstract>, 10.1093/treephys/27.3.413, 2007.
- White, M. D. and McGrail, B. P.: Stomp (subsurface transport over multiple phase) version 1.0 addendum: Eckechem equilibrium-conservationkinetic equation chemistry and reactive transport, Report, 2005.
- Yeh, G. T., Sun, J., Jardine, P. M., Burgos, W. D., Fang, Y., Li, M. H., and Siegel, M. D.: HYDROGEOCHEM
790 5.0: A Coupled Model of Fluid Flow, Thermal Transport, and HYDROGEO-CHEMical Transport through Saturated-Unsaturated Media: Version 5.0, Report, 2004.

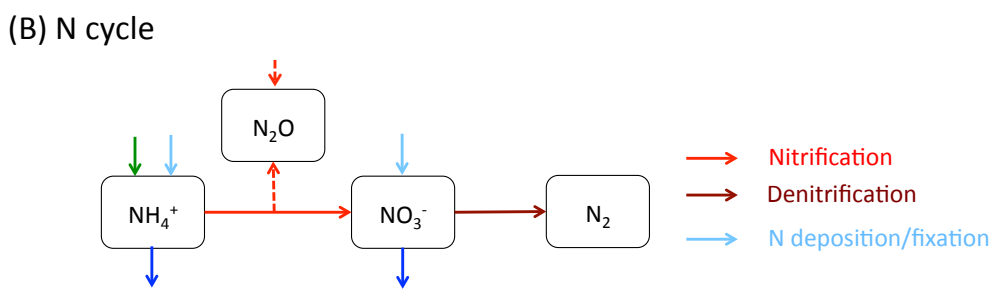
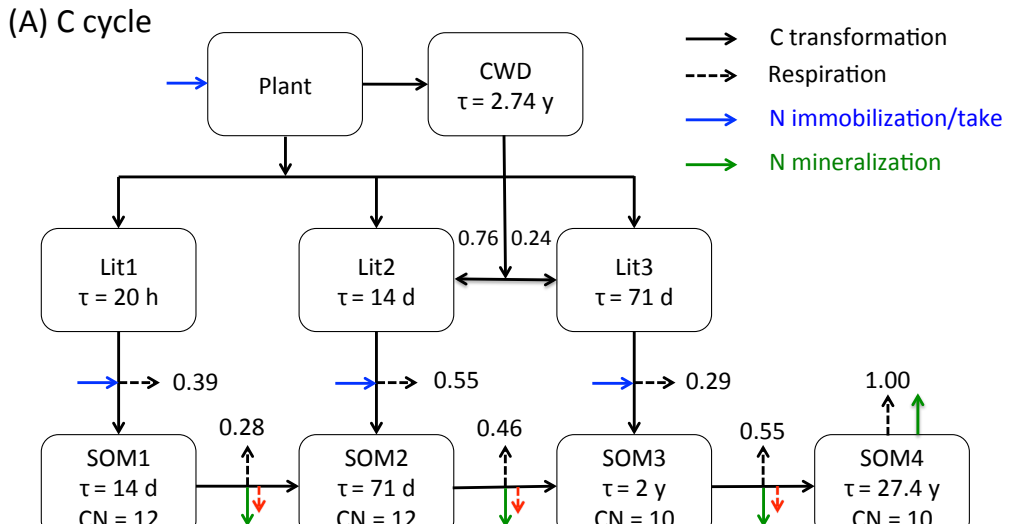


Figure 1. The reaction network for the carbon (A) and nitrogen (B) cycles implemented in this work. The carbon cycle is modified from Thornton and Rosenbloom (2005) and Bonan et al. (2012). τ is the turnover time, and CN is the CN ratio in gC over gN.

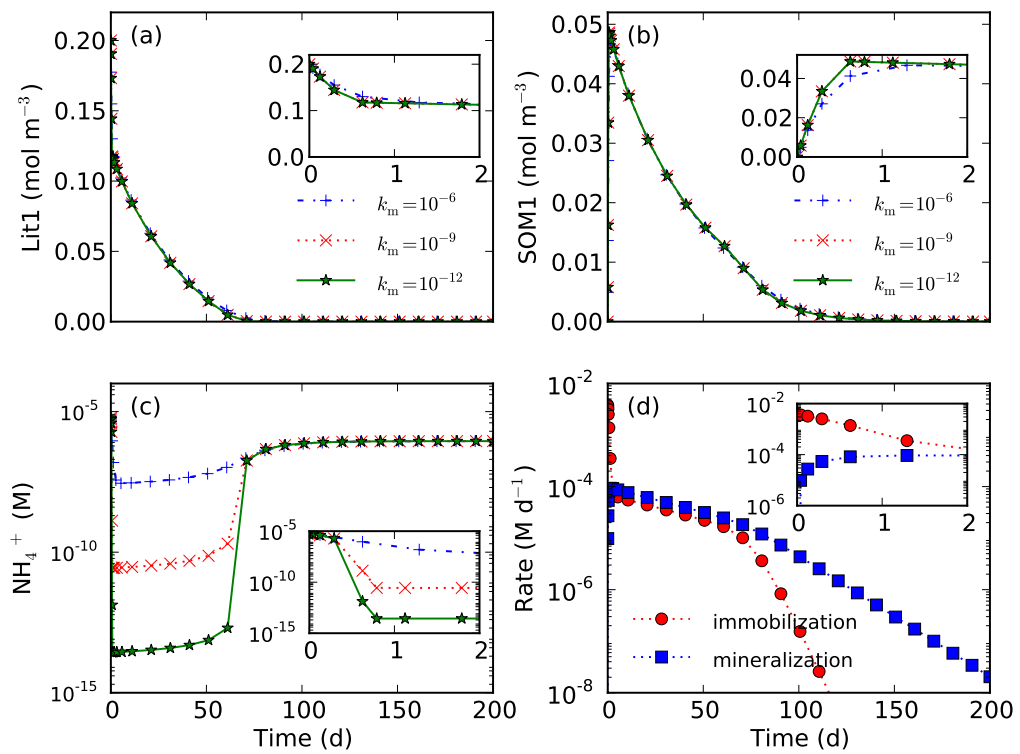


Figure 2. Influence of half saturation k_m on decomposition that involves both nitrogen immobilization and mineralization. Smaller half saturation can result in lower nitrogen concentration (c) but does not substantially impact the calculated concentrations other than ammonium (a, b).

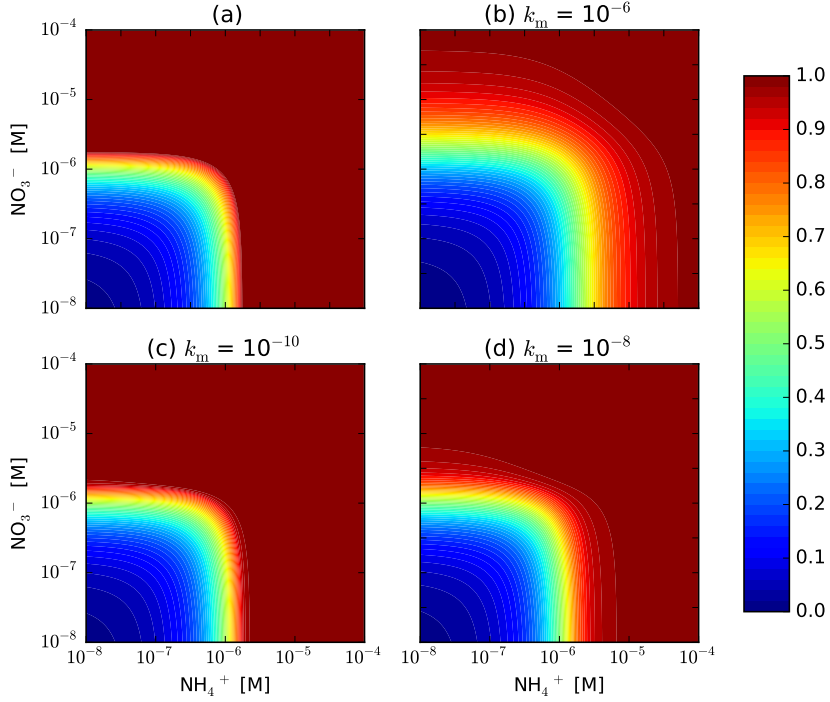


Figure 3. $f_{pi} = \frac{N_{take}}{N_{demand}} = \max\left(1, \frac{[NH_4^+]}{N_{demand}}\right)$ (a) vs. $= \frac{[NH_4^+]}{k_m + [NH_4^+]} + \left(1 - \frac{[NH_4^+]}{k_m + [NH_4^+]}\right) \frac{[NO_3^-]}{k_m + [NO_3^-]}$ (b, c, d) in a 0.5 h time step with an uptake rate of 10^{-9} M s^{-1} . f_{pi} for the latter representation is less than or equal to that for the first one. The difference decreases with decreasing half saturation k_m .

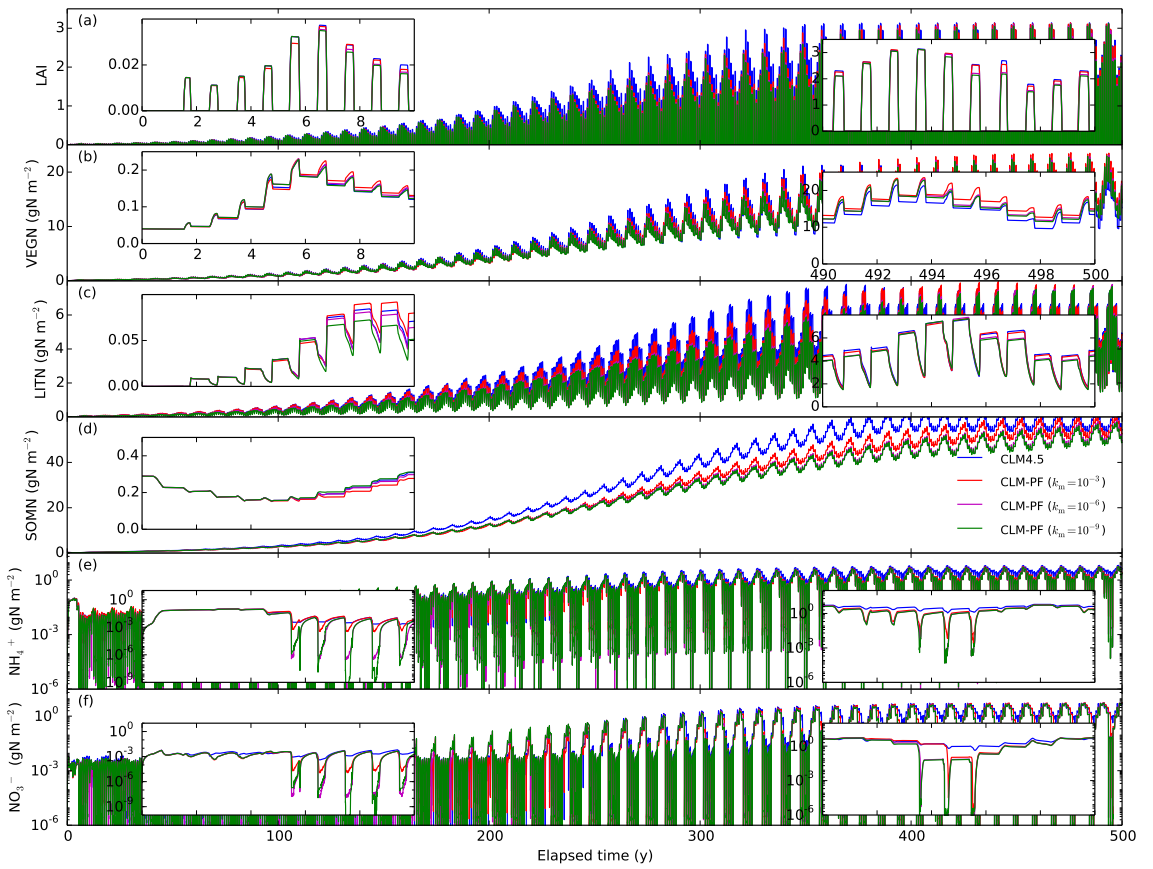


Figure 4. Calculated LAI and nitrogen distribution among vegetation, litter, SOM, NH_4^+ , and NO_3^- pools in spin-up simulations for the US-Brw site.

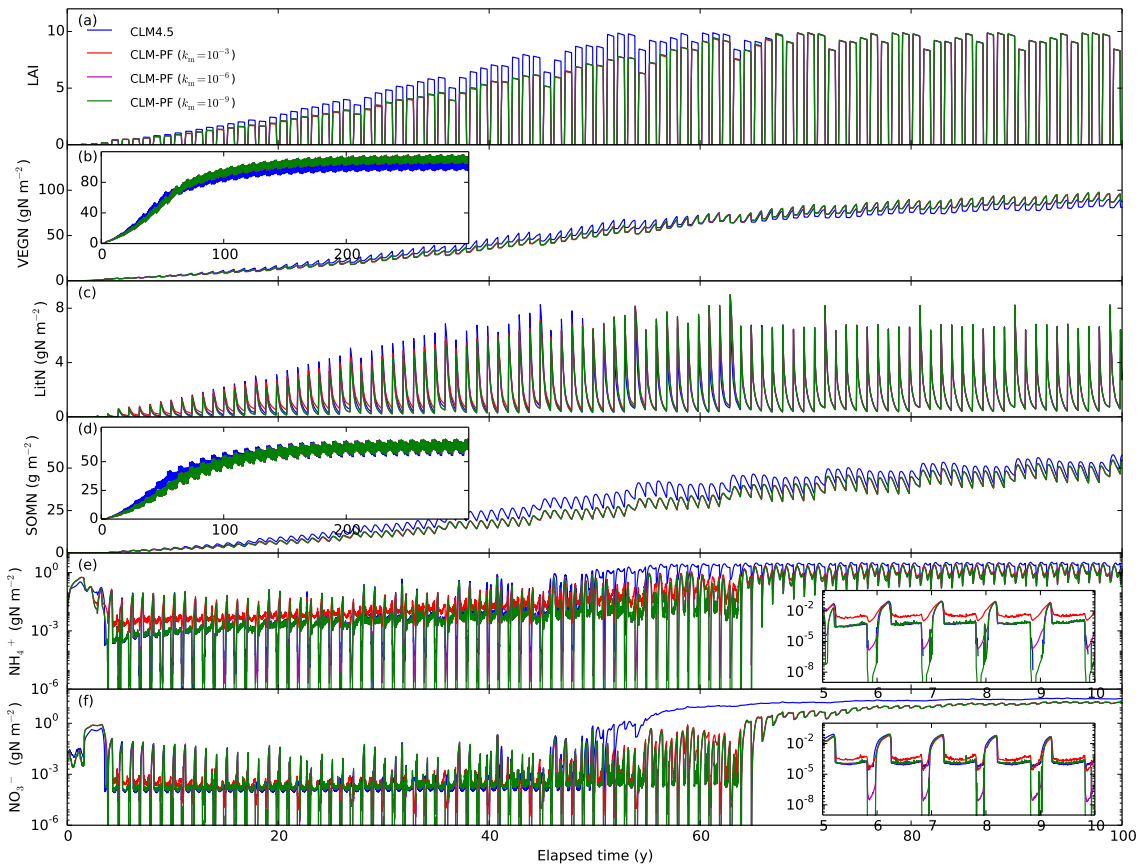


Figure 5. Calculated LAI and nitrogen distribution among vegetation, litter, SOM, NH_4^+ , and NO_3^- pools in spin-up simulations for US-WBW site.

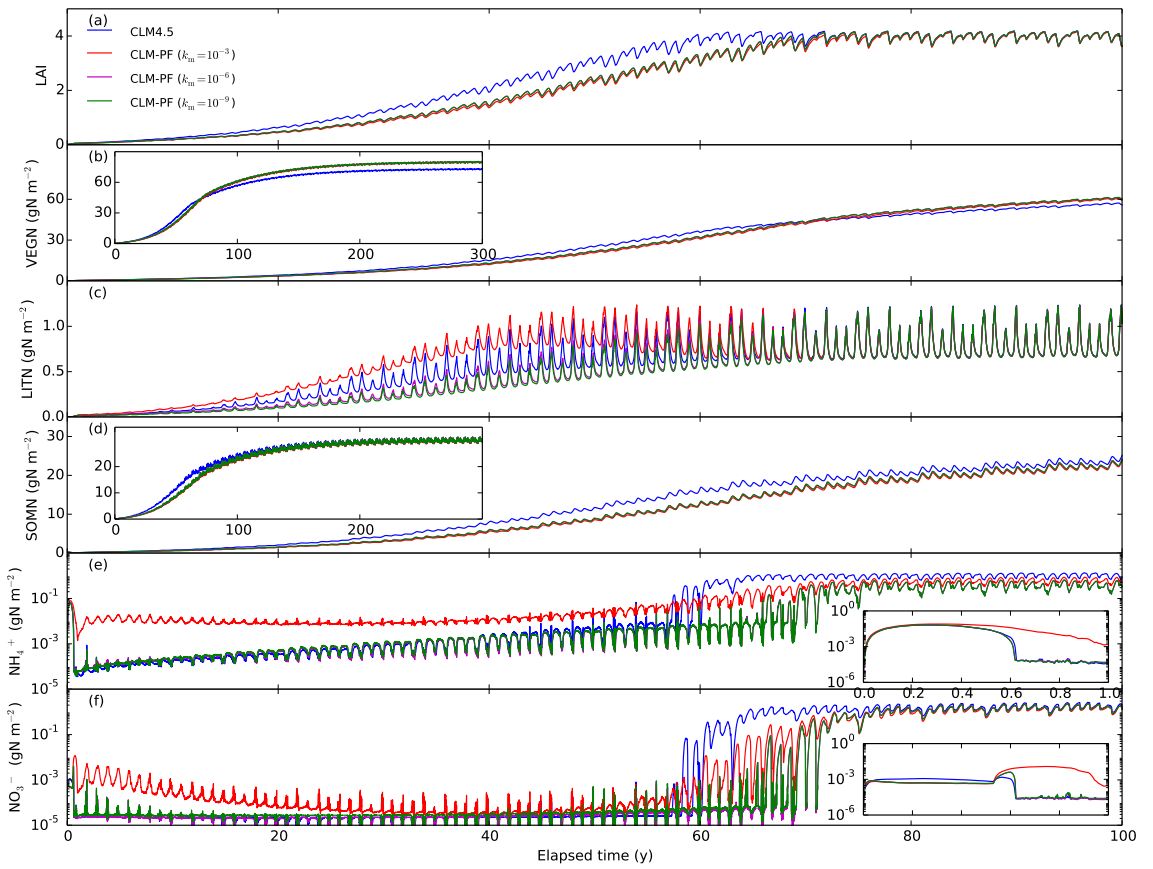


Figure 6. Calculated LAI and nitrogen distribution among vegetation, litter, SOM, NH_4^+ , and NO_3^- pools in spin-up simulations for BR-Cax site.

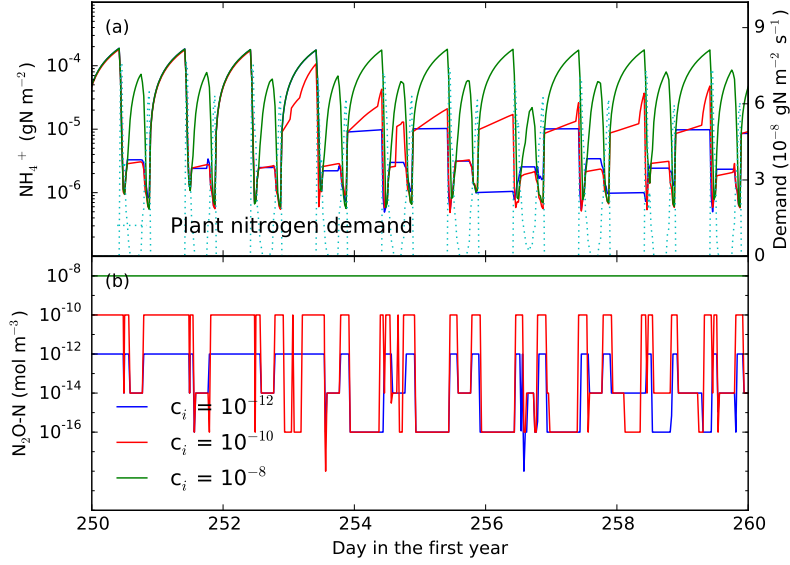


Figure 7. Resetting nitrous oxide concentration to 10^{-8} , 10^{-10} , and 12^{-10} mol m^{-3} in every CLM 0.5 h time step results in no inhibition to increasing inhibition of reactions when the scaling method is used with $\text{STOL} = 10^{-8}$. $\text{N}_2\text{O}-\text{N}$ concentration in the y-axis in (b) is the minimum of the ten soil layers. Numerical experiments are conducted for the tropical site for the first year with $k_m = 10^{-6}$ mol m^{-3} . See inset in Fig. 6(e) for ammonium concentration in the first year with daily data points.

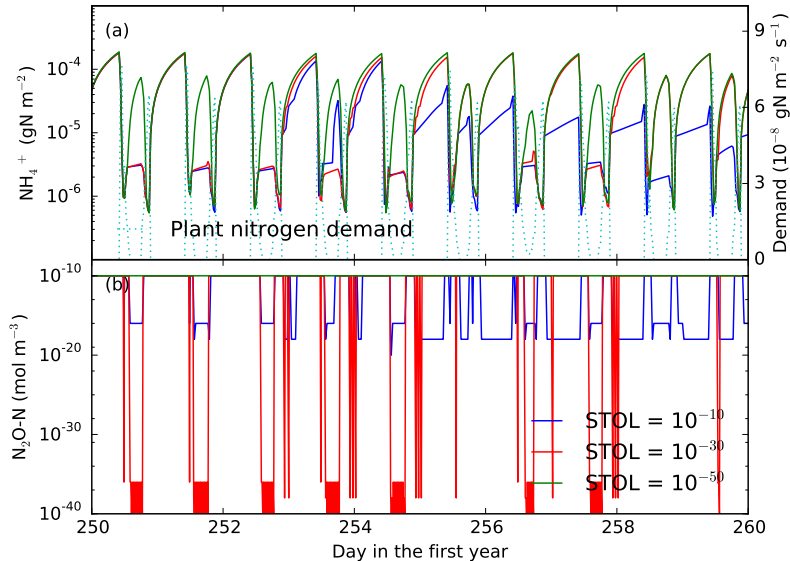


Figure 8. Decreasing STOL can decrease and eliminate the numerical inhibition in the case of $c_i = 10^{-10}$ mol m^{-3} in Fig. 7. $\text{N}_2\text{O}-\text{N}$ concentration in the y-axis in (b) is the minimum of the ten soil layers.

Table 1. Wall time for CLM-PFLOTRAN relative to CLM for spinup simulation on OIC (ORNL Institutional Cluster Phase5)

Site k_m	Clipping			Scaling			Log transformation		
	10^{-3}	10^{-6}	10^{-9}	10^{-3}	10^{-6}	10^{-9}	10^{-3}	10^{-6}	10^{-9}
US-Brw	1.28	1.30	1.30	1.29	1.29	1.32	1.45	1.49	1.72
US-WBW	1.45	1.47	1.47	1.45	1.45	1.47	1.64	1.68	1.89
BR-Cax	1.43	1.49	1.55	1.44	1.48	1.52	1.62	1.66	1.99

CLM wall time is 29.3, 17.7, and 17.1 hours for the Arctic, temperate, and tropical sites for a simulation duration of 1000, 600, and 600 year.

Appendix A: CLM biogeochemical reactions and rates

A1 CLM-CN decomposition

The CLM-CN decomposition cascade consists of three litter pools with variable CN ratios, four soil
795 organic matter (SOM) pools with constant CN ratios, and seven reactions (Bonan et al., 2012; Oleson
et al., 2013; Thornton and Rosenbloom, 2005). The reaction can be described by



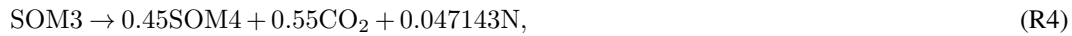
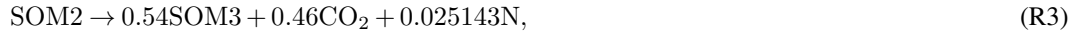
where CN_u and CN_d are the upstream and downstream pools (molecular formula, for 1 mol upstream and downstream pool, there is u and d mol N); N is either NH_4^+ or NO_3^- ; f is the respiration fraction; and $n = u - (1 - f)d$. The rate is
800

$$\frac{d[CN_u]}{dt} = -k_d f_T f_w [CN_u], \quad (A1)$$

where k_d is the rate coefficient, and f_T and f_w are the temperature and moisture response functions.
With a constant CN ratio, the decomposition reactions for the four SOM pools are



805



and



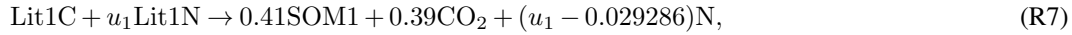
The exact stoichiometric coefficients are calculated in the code using values for respiration factor,
CN ratio, and molecular weight specified in the input file.

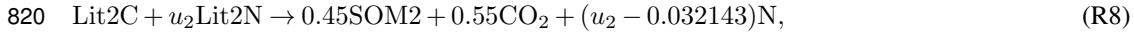
CLM4.5 has an option to separate N into NH_4^+ and NO_3^- . The N mineralization product is NH_4^+ .

As the CN ratio is variable for the three litter pools, litter N pools need to be tracked such that
815 reaction (R1) becomes

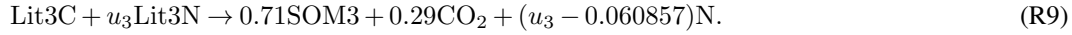


with $u = [LitN]/[LitC]$. The three litter decomposition reactions are





and



As the CN ratio of the litter pools is generally high, u_1 , u_2 , and u_3 are usually small, and n in these reactions (e.g., $n_1 = u_1 - 0.029286$ for Lit1) is normally negative. Namely, these reactions consume
825 (immobilize) N, which can be NH_4^+ , NO_3^- , or both.

A2 Nitrification

The nitrification reaction to produce NO_3^- is



with \dots for additional reactants and products to balance the reaction. The rate is (Dickinson et al.,
830 2002)

$$\frac{d[\text{NH}_4^+]}{dt} = -\frac{d[\text{NO}_3^-]}{dt} = -k_n f_T f_w [\text{NH}_4^+]. \quad (\text{A2})$$

The nitrification reaction to produce N_2O is



with one component related to decomposition as

835 $\frac{d[\text{NH}_4^+]}{dt} = -2\frac{d[\text{N}_2\text{O}]}{dt} = -f_{nm} f_T f_w f_{pH} \max(R_{nm}, 0)$ (A3)

where f_{nm} is a fraction (Parton et al., 1996), and R_{nm} is the net N mineralization rate,

$$R_{nm} = \sum_i n_i R_i, \quad (\text{A4})$$

where R_i denotes the rate of reaction (R2, R3, R4, R5, R7, R8, R9). The second component is (Parton et al., 1996)

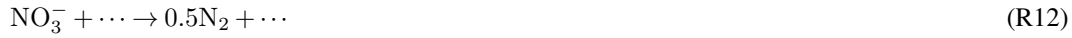
840 $\frac{d[\text{NH}_4^+]}{dt} = -2\frac{d[\text{N}_2\text{O}]}{dt} = -k_{n2o} f_T f_w f_{pH} (1 - e^{-0.0105[\text{NH}_4^+]}).$ (A5)

Ignoring the high-order terms and moving the unit conversion factor into k_{n2o} , it can be simplified as a first-order rate as

$$\frac{d[\text{NH}_4^+]}{dt} = -2\frac{d[\text{N}_2\text{O}]}{dt} = -k_{n2o} f_T f_w f_{pH} [\text{NH}_4^+]. \quad (\text{A6})$$

A3 Denitrification

845 The denitrification reaction is



with rate (Dickinson et al., 2002)

$$\frac{d[\text{NO}_3^-]}{dt} = -2\frac{d[\text{N}_2]}{dt} = -k_{\text{deni}} f_T f_w f_{\text{pH}} [\text{NO}_3^-]. \quad (\text{A7})$$

A4 Plant nitrogen uptake

850 The plant nitrogen uptake reaction can be written as



and



The rate is specified by CLM (plant nitrogen demand) and assumed to be constant in each half-hour
855 time step.

A5 Demand-based competition and demand distribution between ammonium and nitrate

Denote $R_{d,p}$ and $R_{d,i}$ as the potential plant, immobilization, nitrification, and denitrification demand
860 (rate); $R_{a,tot} = R_{d,p} + R_{d,i}$ as the total NH_4^+ demand; and $R_{n,tot}$ as the total NO_3^- demand. CLM
uses a demand-based competition approach to split the available sources in proportion to the demand
rates to meet the demands (Oleson et al., 2013; Thornton and Rosenbloom, 2005). Specifically, for
each time step, if $R_{a,tot}\Delta t \leq [\text{NH}_4^+]$, the uptakes are equal to potential demands, and $R_{n,tot} = 0$;
otherwise, the uptakes for NH_4^+ are $[\text{NH}_4^+]R_{d,p}/R_{a,tot}\Delta t$ and $[\text{NH}_4^+]R_{d,i}/R_{a,tot}\Delta t$ for plants and
immobilization; $R_{n,tot} = R_{a,tot} - [\text{NH}_4^+]/\Delta t$. If $R_{n,tot}\Delta t < [\text{NO}_3^-]$, all of the remaining demand
 $R_{n,tot}$ is met with available NO_3^- . Otherwise, available NO_3^- is split to meet the remaining plant,
865 immobilization, and denitrification demands in proportion to their rates.

Appendix B: Implicit time stepping and Newton-Raphson iteration

Ignoring equilibrium reactions and transport for simplicity of discussion in this work, PFLOTRAN
solves the ordinary differential equation,

$$dc/dt = \mathbf{R}(\mathbf{c}) + \mathbf{F}, \quad (\text{B1})$$

870 where \mathbf{c} is the concentration vector, \mathbf{R} is the kinetic reaction rate, and \mathbf{F} is the fluxes (e.g., nitrogen deposition). Discretizing Eq. (B1) in time using the backward Euler method,

$$(\mathbf{c}^{k+1} - \mathbf{c}^k)/\Delta t = \mathbf{R}(\mathbf{c}^{k+1}) + \mathbf{F}^k. \quad (\text{B2})$$

Solving the equation using the Newton-Raphson method, we denote the residual as

$$\mathbf{f}(\mathbf{c}^{k+1,p}) = (\mathbf{c}^{k+1,p} - \mathbf{c}^k) / \Delta t - \mathbf{R}(\mathbf{c}^{k+1,p}) - \mathbf{F}^k, \quad (\text{B3})$$

875 and Jacobian as

$$\mathbf{J} = \frac{\partial \mathbf{f}(\mathbf{c}^{k+1,p})}{\partial \mathbf{c}^{k+1,p}}, \quad (\text{B4})$$

where p is the iteration counter, the update is

$$\delta \mathbf{c}^{k+1,p+1} = -\mathbf{J}^{-1} \mathbf{f}(\mathbf{c}^{k+1,p}), \quad (\text{B5})$$

and the iteration equation is

$$880 \quad \mathbf{c}^{k+1,p+1} = \mathbf{c}^{k+1,p} + \delta \mathbf{c}^{k+1,p+1}. \quad (\text{B6})$$

The iteration continues until either the residual $\mathbf{f}(\mathbf{c}^{k+1,p+1})$ or the update $\delta \mathbf{c}^{k+1,p+1}$ is less than a specified tolerance. Specifically,

$$\|\mathbf{f}(\mathbf{c}^{k+1,p+1})\|_2 < \text{ATOL}, \quad (\text{B7})$$

$$885 \quad \frac{\|\mathbf{f}(\mathbf{c}^{k+1,p+1})\|_2}{\|\mathbf{f}(\mathbf{c}^{k+1,0})\|_2} < \text{RTOL}, \quad (\text{B8})$$

or

$$\frac{\|\delta \mathbf{c}^{k+1,p+1}\|_2}{\|\mathbf{c}^{k+1,p+1}\|_2} < \text{STOL}. \quad (\text{B9})$$

Here ATOL, RTOL, and STOL are the absolute residual, relative residual, and relative update tolerances. If none of these tolerances are met in MAXIT (the maximum number of iterations before stopping the current iterations) iterations or MAXF (the maximum numb of forward function calls before stopping the current iterations) function evaluations, the iteration is considered to diverge, and PFLOTRAN decreases the time step size for MAX_CUT times. The default values in PFLOTRAN are ATOL = 10^{-50} , RTOL = 10^{-8} , STOL = 10^{-8} , MAXIT = 50, MAXF = 10^4 , and MAX_CUT = 16.

895 Appendix C: Matrix equation for Test 3

Adding to Test 2 a plant NO_3^- uptake reaction (R14) with rate $R_{nt} = R_p \frac{[\text{NH}_4^+]}{[\text{NH}_4^+] + k_m} \frac{[\text{NO}_3^-]}{[\text{NO}_3^-] + k_m}$, $J_{nt,n} = \frac{dR_{nt}}{d[\text{NO}_3^-]} = R_p \frac{[\text{NH}_4^+]}{[\text{NH}_4^+] + k_m} \frac{k_m}{([\text{NO}_3^-] + k_m)^2}$, and $J_{nt,a} = \frac{dR_{nt}}{d[\text{NH}_4^+]} = \frac{dR_p}{d[\text{NH}_4^+]} \frac{k_m}{([\text{NH}_4^+] + k_m)^2} \frac{[\text{NO}_3^-]}{[\text{NO}_3^-] + k_m}$, and a denitrification reaction (R12) with rate $R_{deni} = k_{deni} [\text{NO}_3^-]$, and $J_{deni} = \frac{dR_{deni}}{d[\text{NO}_3^-]} = k_{deni}$, the

matrix equation (Eq. B5) becomes Eq. (C1),

$$\begin{bmatrix} \frac{1}{\Delta t} + J_{at} + J_{nitr} & 0 & 0 & 0 & 0 \\ -J_{at} & \frac{1}{\Delta t} & 0 & 0 & 0 \\ -J_{nitr} + J_{nt,a} & 0 & \frac{1}{\Delta t} + J_{nt} + J_{deni} & 0 & 0 \\ -J_{nt,a} & 0 & -J_{nt,n} & 1/\Delta t & 0 \\ 0 & 0 & -0.5J_{deni} & 0 & 1/\Delta t \end{bmatrix} \begin{pmatrix} \delta[\text{NH}_4^+]^{k+1,1} \\ \delta[\text{PlantA}]^{k+1,1} \\ \delta[\text{NO}_3^-]^{k+1,1} \\ \delta[\text{PlantN}]^{k+1,1} \\ \delta[\text{N}_2]^{k+1,1} \end{pmatrix} = - \begin{pmatrix} R_{at} + R_{nitr} \\ -R_{at} \\ -R_{nitr} + R_{nt} + R_{deni} \\ -R_{nt} \\ -0.5R_{deni} \end{pmatrix}. \quad (\text{C1})$$

900